

ORIGINAL ARTICLE

N^6 -methyladenosine-regulated exosome biogenesis orchestrates an immunosuppressive pre-metastatic niche in gastric cancer peritoneal metastasis

Song Li¹ | Jianyuan Zhou¹ | Shuang Wang¹ | Qian Yang¹ | Shulun Nie¹ | Chunwang Ji¹ | Xue Zhang^{1,2} | Shuhan Li¹ | Xuanyu Zhou¹ | Jiahui Chu³ | Xuehui Wu¹ | Jianqiao Jiao¹ | Ruitao Xu¹ | Qian Xu¹ | Miao Huang¹ | Qiushi Wang¹ | Liliang Dou¹ | Qin Qin Hu¹ | Fan Jiang¹ | Xin Dai^{1,4} | Zhaodi Nan¹ | Xinyu Song¹ | Di Zhang¹ | Lian Liu¹ 

¹Department of Medical Oncology, Qilu Hospital, Cheeloo College of Medicine, Shandong University, Jinan, Shandong, P. R. China

²Institute of Marine Science and Technology, Shandong University, Qingdao, Shandong, P. R. China

³Department of Pharmacy, Qilu Hospital, Cheeloo College of Medicine, Shandong University, Jinan, Shandong, P. R. China

⁴Department of Medical Oncology, Shandong Provincial Hospital of Traditional Chinese Medicine, Jinan, Shandong, P. R. China

Correspondence

Lian Liu, MD, PhD, Department of Medical Oncology, Qilu Hospital, Cheeloo College of Medicine, Shandong University, Jinan 250012, Shandong, P. R. China.

Email: lianliu@sdu.edu.cn

Funding information

National Natural Science Foundation of China, Grant/Award Number: 82173305;

Abstract

Background: Gastric cancer peritoneal metastasis is clinically challenging, given the limited treatment options and poor prognosis. The molecular mechanisms that precede gastric cancer peritoneal metastasis, known as the pre-metastatic niche (PMN), and its relationship with N^6 -methyladenosine (m^6A) modification remain unclear.

Methods: We used 87 resected gastric cancer tissues and 4 public datasets to explore the association between methyltransferase-like 3 (METTL3) expres-

List of abbreviations: ACRG, Asian Cancer Research Group; ACT, annotation of cell types; ANOVA, analysis of variance; CFSE, carboxyfluorescein succinimidyl ester; EBV, Epstein-Barr virus; EDTA, ethylenediaminetetraacetic acid; EDM, exosome-depleted media; ELISA, enzyme-linked immunosorbent assay; FACS, fluorescence-activated cell sorting; FDR, false discovery rate; GFP, green fluorescent protein; IL, interleukin; isPMN, immunosuppressive pre-metastatic niche; m^6A , N^6 -methyladenosine; METTL3, methyltransferase-like 3; *METTL3*-cd, catalytically dead METTL3; *METTL3*-oe, *METTL3*-overexpressed; *METTL3*-oe-exo, *METTL3*-overexpressed cell-derived exosome; MDSC, myeloid-derived suppressor cell; MIR17PTi, MIR17HG primary transcript inhibitor; MSI-H, microsatellite instability-high; NF- κ B, nuclear factor-kappa B; NK, natural killer; NTA, nanoparticle tracking analysis; PBS, phosphate-buffered saline; PKH, Paul Karl Horan; PLC, peritoneal lavage cells; PMN, pre-metastatic niche; qPCR, quantitative polymerase chain reaction; RAB27A, ras-related protein Rab-27A; RIP, RNA immunoprecipitation; RNA-seq, RNA sequencing; RPMI, Roswell Park Memorial Institute; scRNA-seq, single-cell RNA sequencing; SRCIN1, SRC kinase signaling inhibitor 1; siRNA, small interfering RNA; SRC, SRC proto-oncogene, non-receptor tyrosine kinase; STR, short tandem repeat; TCGA, The Cancer Genome Atlas; TGF- β , transforming growth factor- β ; TNF, tumor necrosis factor; t-SNE, t-distributed stochastic neighbor embedding; UTR, untranslated region; YTHDF1, YTH N^6 -methyladenosine RNA binding protein F1.

Song Li, Jianyuan Zhou, Shuang Wang, and Qian Yang contributed equally to this study.

This is an open access article under the terms of the [Creative Commons Attribution-NonCommercial-NoDerivs](https://creativecommons.org/licenses/by-nc-nd/4.0/) License, which permits use and distribution in any medium, provided the original work is properly cited, the use is non-commercial and no modifications or adaptations are made.

© 2025 The Author(s). *Cancer Communications* published by John Wiley & Sons Australia, Ltd. on behalf of Sun Yat-sen University Cancer Center.

Natural Science Foundation of Shandong Province, Grant/Award Number: ZR2023LSW018

sion and gastric cancer peritoneal metastasis. Roles of m⁶A, exosomes, or macrophages in PMN formation were explored in immunocompetent mouse models through exosome treatments or macrophage modifications. Key genes and regulatory mechanisms were uncovered using mass spectrometry, RNA/miRNA sequencing, RNA-immunoprecipitation, dual-luciferase assays, and point mutations in the ras-related protein Rab-27A (*RAB27A*) in cells. Macrophage and T-cell functions were assessed using enzyme-linked immunosorbent assay, flow cytometry, and cytotoxicity assays.

Results: METTL3 overexpression in gastric cancer cells enhanced *RAB27A* translation by methylating its mRNA A502 base, facilitated by its m⁶A “reader” YTH N⁶-methyladenosine RNA binding protein F1 (YTHDF1), and led to increased exosome biogenesis. The miRNA-17-92 cluster was enriched in METTL3-overexpressed cell-derived exosomes and targeted SRC kinase signaling inhibitor 1 (*SRCIN1*) to activate SRC proto-oncogene, non-receptor tyrosine kinase (SRC) signaling in peritoneal macrophages. Macrophage activation skewed cytokine production towards an immunosuppressive profile in the peritoneum, elevating the levels of interleukin (IL)-10 and tumor necrosis factor (TNF) and reducing the levels of IL-1 and IL-6. These cytokine shifts inhibited T cell proliferation and cytotoxic activities, which created an immunosuppressive PMN and led to peritoneal metastasis. The association between METTL3, macrophages, and peritoneal metastasis was verified in clinical samples.

Conclusions: Our study identified an intricate m⁶A-regulated mechanism of peritoneal PMN development that is mediated by exosome-promoted macrophages. These insights into gastric cancer peritoneal metastasis offer promising directions for translational research.

KEYWORDS

exosomes, gastric cancer, N⁶-methyladenosine, peritoneal metastasis, pre-metastatic niche

1 | BACKGROUND

Gastric cancer is among the most prevalent types of cancer worldwide, ranking fifth in incidence and fourth in mortality [1]. Typically asymptomatic at early stages, approximately 40% of gastric cancer cases are diagnosed with distant metastasis [2]. Peritoneal metastasis is the most common type of metastasis, accounting for 61%–80% of all gastric cancer cases [3]. Even after radical surgery, 10%–46% of patients develop peritoneal metastases [4]. Although systemic and intraperitoneal therapies have been widely used [5], their outcomes are far from satisfactory. Systemic treatments only yield a median survival of 3 to 6 months, whereas the efficacy of local therapies remains uncertain and controversial [6]. To improve survival rates, we need to better understand the mechanisms accounting for gastric cancer peritoneal metastasis so that we may develop more effective prevention and treatment strategies.

The recent theory of pre-metastatic niches (PMN) has shed light on the initial phases of tumor metastasis [7]. A primary tumor induces a supportive microenvironment at a specific distant site to prepare for colonization by altering the local nutrients, extracellular matrix, stromal cells, and immune responses [8]. Immunosuppression is a key feature of PMN, wherein the primary tumor remotely mobilizes immunosuppressive cells (such as myeloid-derived suppressor cells [MDSCs] and macrophages), inhibits immune response cells (such as CD8⁺ T lymphocytes and natural killer [NK] cells), disrupts the balance between inflammatory and anti-inflammatory cytokines, activates complement cascades, and induces immune checkpoint expression [9–10]. However, the immunological characteristics and role of PMN in gastric cancer peritoneal metastasis are not well defined.

To form PMN, primary tumors secrete soluble molecules that modulate the local microenvironment at potential metastatic sites [11]. Among these factors, exosomes

are critical because they can carry diverse biomolecules (including DNA, RNA, proteins, and lipids), efficiently transmit core information to distant sites, and foster immunosuppressive PMN (isPMN) [12]. Specifically, exosomes have been shown to polarize tumor-associated macrophages and neutrophils, inhibit dendritic cell maturation, induce regulatory T cell differentiation, and recruit MDSCs [13]. However, whether isPMN-inducing exosomes exist and function in gastric cancer peritoneal metastasis remains unclear.

N^6 -methyladenosine (m^6A), an epigenetic modification, is the most prevalent RNA modification in eukaryotic cells and has emerged as a central player in numerous aspects of cancer pathogenesis, including cancer stem cell renewal and differentiation, treatment resistance, tumor microenvironment modulation, tumor immune evasion, and regulation of tumor metabolism [14]. Previously, we identified methyltransferase-like 3 (*METTL3*), an m^6A “writer,” as a pivotal factor in promoting gastric cancer development and peritoneal metastasis by expediting miR-17-92 cluster biogenesis and activating the protein kinase B (Akt)/mammalian target of rapamycin (mTOR) pathway in a nude mouse model [15]. *METTL3* also suppresses basic leucine zipper ATF-like transcription factor 2 (*BATF2*) [16] and intermediate filament family orphan 1 (*IFFO1*) [17] expression by m^6A modification, promoting gastric cancer cell growth in the peritoneal cavity of nude mice. Although these studies provided initial insights into *METTL3*'s significance in gastric cancer progression, the lack of a complete immune system in nude mouse models restricted the understanding of the immune characteristics of peritoneal PMN and of the tumor microenvironment in gastric cancer peritoneal metastasis. To date, the relationship between m^6A modification in mRNA of gastric cancer cells and peritoneal PMN remains to be fully explored.

In this study, we established a gastric cancer peritoneal metastasis model using immunocompetent mice to reveal the presence of isPMN prior to the onset of gastric cancer peritoneal metastasis and to investigate its regulators. We found that *METTL3* is crucial for generating isPMN within the peritoneal cavity by regulating exosome biogenesis and its cargo. This study provides insights to the intricate steps of this process, including how *METTL3* controls exosomes, the characteristics of exosome-induced PMN formation, and how isPMN supports peritoneal metastasis.

2 | MATERIALS AND METHODS

2.1 | Cell culture and transfection

Human gastric cancer AGS and MKN-45 cell lines were obtained from the Cell Bank of the Chinese Academy

of Sciences (Shanghai, P. R. China). A mouse forestomach carcinoma (MFC) cell line, capable of growing in immunocompetent 615 mice [18] and widely used in cancer immunology studies [19, 20], and MFC-expressing luciferase (MFC-LUC) cells were acquired from Shanghai Zhong Qiao Xin Zhou Biotechnology Co., Ltd. (Shanghai, P. R. China). RAW 264.7 cells were obtained from Procell Life Science & Technology (Wuhan, Hubei, P. R. China). 293T cells were generously provided by Dr. Jianjun Xie from Shantou University (Guangdong, P. R. China). All cell lines were authenticated by short tandem repeat (STR) profiling and were routinely screened for mycoplasma contamination using quantitative polymerase chain reaction (qPCR). AGS and MKN-45 cells were cultured in Dulbecco's Modified Eagle Medium (KGL1211-500, Jiangsu KeyGEN BioTECH, Nanjing, Jiangsu, P. R. China), while MFC cells were in Roswell Park Memorial Institute (RPMI) 1640 medium (KGL1506-500, Jiangsu KeyGEN BioTECH). Both of them were supplemented with 10% fetal bovine serum (FBSAD-01011-500, OriCell, Santa Clara, CA, USA) and 1% penicillin/streptomycin (P1400, Solarbio, Beijing, P. R. China).

Lipofectamine 3000 (L3000015, Thermo Fisher Scientific, Waltham, MA, USA) was used for plasmid, miRNA mimic, and miRNA inhibitor transfection in AGS, MKN-45, 293T, and MFC cells. Lipofectamine RNAiMAX (13778150, Thermo Fisher Scientific) was used for siRNA transfection in AGS cells. Lentiviruses (GeneChem, Shanghai, P. R. China) were produced in 293T cells, followed by puromycin selection for stable cell line generation using target genetic constructs.

2.2 | Plasmid construction

Overexpression plasmids, lentiviruses, and shRNA for *METTL3* have been previously described [21]. Catalytically dead *METTL3* (*METTL3*-cd, *METTL3* with D394A, and W397A mutations) was cloned into the overexpression vector as previously described [22]. Full-length human ras-related protein Rab-27A (*RAB27A*) was cloned into the GV658 vector for overexpression studies and specific point mutations were introduced as required. For lentiviruses overexpressing *mettl3*, full-length *mettl3* sequences were inserted into a GL122 vector. Lentiviruses containing nucleotides 965-1914 of microRNA 17 host gene (*Mir17hg*) were cloned into a GL132 vector. For sphingomyelin phosphodiesterase 3 (*Smpd3*) knockdown, shRNA sequences were inserted into a GL428 vector. The 3' untranslated region (UTR) of *SRC kinase signaling inhibitor 1* (*Srcin1*) was cloned into the pmirGLO dual-luciferase miRNA target expression vector for luciferase reporter gene assays. siRNAs targeting *RAB27A* were synthesized by RiboBio

(Guangzhou, Guangdong, P. R. China). Small RNAs used in this study are listed in Supplementary Table S1.

2.3 | Exosome isolation

AGS, MKN-45, or MFC cells were maintained in serum-free media for 48 h, respectively. The collected supernatant was centrifuged sequentially (300 ×g for 10 min, 2,000 ×g for 10 min, 10,000 ×g for 30 min, 100,000 ×g for 70 min). The post-centrifugation supernatant was designated as the de-exosome fraction. The exosome pellet was resuspended in phosphate-buffered saline (PBS) and centrifuged (100,000 ×g for 70 min) to purify the exosome samples. Ascites samples from patients with gastric cancer peritoneal metastasis were subjected to exosome isolation using the exoEasy Maxi kit (E1002, QIAGEN, Duesseldorf, Germany), following the manufacturer's instructions. The size and morphology of the isolated exosomes were characterized using electron microscopy (JEM-1200EX, JEOL, Tokyo, Japan).

2.4 | Clinical sample collection

Formalin-fixed, paraffin-embedded gastric cancer tissues from 87 patients collected between 2009 and 2014 were obtained from the Department of Pathology, Shandong University Qilu Hospital (Shandong, P. R. China), as previously described [15]. All tissue samples were obtained from surgery, including 66 cases of radical gastrectomy and 21 cases of palliative gastrectomy. Ascites samples were collected from 12 patients with gastric cancer-associated malignant ascites or cirrhosis-associated ascites who underwent peritoneocentesis for clinical management at the Departments of Medical Oncology and the Departments of Hepatology, Shandong University Qilu Hospital. Ascites samples were then centrifuged (3,000 rpm for 10 min), aliquoted, and stored at -80°C for subsequent analyses.

2.5 | Immunohistochemistry staining

Tissue sections were prepared, incubated at 60°C, deparaffinized in xylene, and rehydrated through graded alcohols. Antigen retrieval was carried out using ethylenediaminetetraacetic acid (EDTA) buffer (ZLI-9071, Zsbio, Beijing, P. R. China), followed by blocking with goat serum (SP-9001-2, Zsbio). The sections were then incubated with an anti-METTL3 antibody (ab195352, Abcam, Cambridge, UK; 1:2000 dilution) using the immunohistochemistry kit (SP-9001, Zsbio). Hematoxylin was used for nuclear coun-

terstaining. METTL3 staining intensity was evaluated by three independent researchers and graded as negative (-), weak (+), moderate (++) or strong (+++). Tumors with (-) and (+) staining were classified as METTL3-low, whereas those with (++) and (+++) staining were classified as METTL3-high.

2.6 | Mouse model

Male 615 mice (aged 6-8 weeks) were procured from the Institute of Hematology, Chinese Academy of Medical Sciences (Beijing, P. R. China) and housed at the Animal Center of Shandong University Qilu Hospital. All experimental procedures were approved by the Ethics Committee on Animal Experiments of Shandong University Qilu Hospital (No. DWLL-2022-069) and conformed to the ARRIVE guidelines [23]. All experimental interventions were performed during the light cycle.

To establish the peritoneal metastasis model, 1×10^6 MFC or MFC-LUC cells were intraperitoneally injected, respectively. Abdominal circumference and body weight were recorded every 3 days. Bioluminescence from MFC-LUC cells was measured every 5 days. Animals were euthanized 16 days post-injection for the assessment of ascites and nodule number.

For peritoneum "education" experiments, conditioned serum-free media or exosome-depleted serum-free media from MFC cells was concentrated at a ratio of 50:1 using an Amicon Ultra-15 Centrifugal Filter Unit with Ultracel-10 membrane (MWCO = 3 kDa; Merck Millipore, Billerica, MA, USA). Concentrated conditioned media (200 μL) or MFC-derived exosomes (20 μg/200 μL) was administered intraperitoneally to 615 mice every other day for 10 days.

Peritoneal lavage cells (PLC) and macrophages were extracted as previously described [24]. For the peritoneal lavage cell transfer model, exosome-treated mice were humanely sacrificed, limbs were fixed, and abdomens were sterilized using 70% ethanol. Using sterile scissors, the peritoneal cavity was exposed, and 5 mL of cold normal saline was injected intraperitoneally, followed by gentle massage. Ascites was carefully extracted to prevent organ damage. PLC were resuspended in saline and injected into recipient mice.

For the macrophage transfer model, PLC were extracted from untreated mice as described above. These cells were cultured in RPMI 1640 medium for 2 h to allow macrophage adherence. Non-adherent cells were removed, and adherent macrophages were subsequently treated with exosomes for 24 h. These exosome-treated macrophages were collected and injected intraperitoneally into recipient mice at five-day intervals starting from the initial administration of MFC cells until euthanasia.

For the macrophage depletion model, mice received intraperitoneal injections of clodronate liposomes or control liposomes (F70101C-NC, FormuMax Scientific, CA, USA) at five-day intervals until euthanasia (initial dose 1.4 mg, subsequent doses 0.7 mg).

2.7 | Exosome tracing

Exosomes were labeled with Paul Karl Horan (PKH)-67 dye (UR52303, Umibio, Shanghai, China) by incubating 100 μ L of exosomes with 50 μ L of 100 μ M PKH-67 for 10 min. Labeled exosomes (20 μ g) were administered intraperitoneally every other day for a total of 5 doses. Following the last injection, mice were anesthetized, and ascitic cells were collected with 5 mL of cold saline. The uptake of PKH-67-labeled exosomes by immune cells was analyzed using flow cytometry.

2.8 | Tumor-peritoneum adhesion assay

To facilitate digestion, mice were anesthetized, injected intraperitoneally with 5 mL of 0.25% Trypsin/EDTA Solution (CSP087, Shanghai Zhong Qiao Xin Zhou Biotechnology), and incubated for 25 min. Digestion was then terminated by adding 1 mL of 10% fetal bovine serum into the peritoneal cavity. The peritoneal fluid was aspirated using a syringe (yielding approximately 5 mL) and centrifuged (500 \times g, 70 min). The supernatant was discarded, and the cells were resuspended and adjusted to a concentration of 1×10^5 cells/mL. The purity of mesothelial of >90% was confirmed by immunofluorescence using anti-Vimentin and E-cadherin antibodies. Once the cells formed a confluent monolayer, MFC overexpressing green fluorescent protein (MFC-GFP) cells, along with exosomes or PLC, were transferred to the plates and incubated for 24 h. Non-adherent cells were gently removed by washing with PBS. Cell adhesion was observed and recorded under an Invitrogen EVOS FL Auto 2 microscope (Thermo Fisher Scientific).

2.9 | Polysome profiling

AGS cells were treated with 100 μ g/mL cycloheximide (HY-12320, MedChemExpress, Shanghai, P. R. China) at 37°C for 8 min before being lysed in 1 mL of buffer containing 15 mmol/L Tris-HCl (pH 7.5), 200 mmol/L NaCl, 15 mmol/L MgCl₂, 1% Triton X-100, 100 μ g/mL cycloheximide, 1 \times protease inhibitor cocktail (HY-K0010, MedChemExpress), and 40 U/mL RNase inhibitor (HY-K1033, MedChemExpress). The lysate was centrifuged

(12,000 \times g, 10 min, 4°C). The resulting supernatant was then gently layered onto a sucrose gradient and centrifuged using a Beckman SW41Ti rotor (36,000 rpm, 3 h, 4°C; optima XPN-100, Beckman Coulter, Miami, FL, USA). Fraction separation was performed using a density gradient fractionation system (152-002, BioComp, Fredericton, NB, Canada). RNA was extracted using TRIzol (15596026CN, Invitrogen, Waltham, MA, USA).

2.10 | qPCR

Total RNA was extracted using the EasyPure Fast Cell RNA Kit (ET111-01-V2, TransGen Biotech, Beijing, P. R. China), reverse-transcribed with HiScript III RT Super-Mix (R323-01, Vazyme, Nanjing, Jiangsu, P. R. China), and quantified using ChamQ Universal SYBR qPCR Master Mix (Q341-02, Vazyme). miRNA quantification was performed using an All-in-One miRNA qRT-PCR Detection Kit (QP115, GeneCopoeia, San Diego, CA, USA). Primer sequences are detailed in Supplementary Table S2.

2.11 | Western blotting

Cells were lysed on ice using radio-immunoprecipitation assay buffer supplemented with the cComplete™ Protease Inhibitor Cocktail (11697498001, Roche, Billerica, MA, USA). Protein concentration was quantified using a BCA Protein Assay Kit (KTD3001, Abbkine Biotechnology, Wuhan, Hubei, P. R. China). Approximately 25 μ g of protein were separated by sodium dodecyl sulfate-polyacrylamide gel electrophoresis and transferred onto a 0.22 μ m polyvinylidene difluoride membrane (88520, Thermo Fisher Scientific). Membranes were blocked with Normal Goat Serum (SL038, Solarbio) and probed with primary antibodies. Blots were developed using horseradish peroxidase-conjugated secondary antibodies and enhanced chemiluminescence (WBULP-100ML, Merck Millipore), then visualized using a digital imaging system (SinSage Technology, Beijing, P. R. China). The antibodies used are listed in Supplementary Table S3 and were diluted according to the manufacturers' instructions using Universal Antibody Diluent Buffer (BMU103, Abbkine Biotechnology).

2.12 | Enzyme-linked immunosorbent assay (ELISA)

Mouse cytokines interleukin (IL)-10 (MM-0176M2), IL-6 (MM-0163M2), transforming growth factor- β (TGF- β ; MM-0689M2), and IL-1 (MM-0040M2); and human cytokines

IL-10 (MM-0066H1), TGF- β (MM-63141H1), and IL-6 (MM-0049H1) were detected using ELISA kits (Jiangsu Meimian, Yancheng, Jiangsu, P. R. China) according to the manufacturer's protocols.

2.13 | Flow cytometry

Cell viability was determined using Zombie NIR dye (423101, BioLegend, San Diego, CA, USA), with non-specific immunofluorescent staining minimized using an Fc receptor-blocking reagent (130-092-575, Miltenyi Biotec, Auburn, CA, USA). The cells were treated with a fixation/permeabilization solution kit (554714, BD Biosciences, San Jose, CA, USA) according to the guidelines for intracellular staining. Following antibody staining, the cells were washed, resuspended, and sieved through a 100 μ m nylon mesh before acquisition. Data were collected using a FACSCalibur flow cytometer (Gallios B47904, Beckman Coulter) and analyzed using FlowJo software (v10.8.1, TreeStar Inc., Ashland, OR, USA).

2.14 | Nanoparticle tracking analysis (NTA)

Exosomal particles were resuspended, brought to a suitable concentration (2×10^8 to 1×10^9 particles/mL), and analyzed using a NanoSight NS300 Nanoparticle Tracking Analyzer (Malvern Instruments Ltd., Worcestershire, UK), which features a 488 nm laser and a highly sensitive sCMOS camera. The NanoSight NTA software (Version 2.3, Malvern Instruments Ltd.) was used to quantify particles precisely.

2.15 | RNA immunoprecipitation (RIP)

RNA-binding proteins were immunoprecipitated using a Magna RIP RNA-Binding Protein Immunoprecipitation Kit (17-700, Merck Millipore) with antibodies against YTH N^6 -methyladenosine RNA binding protein F1 (YTHDF1), METTL3, and m^6A . Co-precipitated RNA was quantified by qRT-PCR using primers specific for *RAB27A*. Total RNA and isotype IgG served as input and negative controls, respectively.

2.16 | Reverse RNA pull-down

Biotinylated *RAB27A* RNA probes (5'-3' direction: ACCGTTCCATTTCGCTTCATTATCAG) were conjugated to streptavidin-coated magnetic beads using a PierceTM Magnetic RNA-Protein pull-down kit (20164, Thermo

Fisher Scientific). The beads were then introduced into the cellular lysates and incubated to allow for interactions. After incubation, the non-bound components were removed using a washing buffer, and the captured proteins were eluted for Western blotting analysis.

2.17 | Actinomycin D and anisomycin treatment

We seeded 1.2×10^6 cells into six-well plates and cultured them until they reached 60% confluence. For the actinomycin D assay, cells were treated with 10 μ g actinomycin D (MB2221, MeilunBio, Dalian, Liaoning, P. R. China) and then harvested (0, 1, 2, 4, 6, and 8 h post-treatment) for qPCR analysis. For the anisomycin assay, cells were treated with 3 μ mol/L anisomycin (HY-18982, MedChemExpress, Monmouth Junction, NJ, USA) for 8 h before lysis and Western blotting analysis.

2.18 | Dual-luciferase reporter assay

293T cells were transfected with dual-luciferase vectors harboring the 3'UTR of *Srcin1* or its mutated sequence, by replacing the target sequence of miR-17-5p and miR-20a-5p with its antisense counterparts, in conjunction with miR-17-5p or miR-20a-5p mimics or inhibitors (RiboBio). Luciferase activity was quantified 48 h post-transfection using a Duo-Lite Luciferase Assay System (DL101, Vazyme) and detected using a microplate reader (INFINITE M200, Tecan, Mannedorf, Switzerland).

2.19 | Treatment of exosomes on macrophages

RAW 264.7 cells were cultured for 24 h in an exosome-free conditioned medium. After the initial 24-hour incubation, the medium was replaced with fresh conditioned media containing exosomes (20 μ g/mL) or an equivalent volume of PBS. The cells were then cultured for an additional 2-5 days to assess proliferation, macrophage markers, mRNA sequencing (mRNA-seq), and cytokine production.

2.20 | T-cell isolation and proliferation assay

To isolate T lymphocytes, spleens were homogenized and subjected to red blood cell lysis to prepare a single-cell suspension. Total T lymphocytes were isolated using a Pan T Cell Isolation Kit II (130-095-130, Miltenyi Biotec,

Bergisch Gladbach, North Rhine-Westphalia, Germany). Following isolation, cells were labeled with CellTrace™ carboxyfluorescein succinimidyl ester (CFSE, 65-0850-84, Invitrogen) and stimulated with Dynabeads® Mouse T-Activator CD3/CD28 for T-Cell Expansion and Activation (11453D, Gibco, Waltham, MA, USA) and Mouse IL-2 Recombinant Protein (50 ng/mL; 212-12, PeproTech, Rocky Hill, NJ, USA). After treatment with exosomes or co-culture with macrophages pretreated with exosomes or overexpressing miR-17-92 cluster using Transwell compartments (six-well plate; Corning, NY, USA), the expanded T lymphocytes were harvested, and their proliferation was evaluated using flow cytometry after 72 h.

2.21 | T cell killing assay

T lymphocytes were co-cultured with MFC-GFP cells in a six-well plate, with RAW 264.7 cells in the upper chamber. Following a three-day incubation, MFC-GFP cells were visualized using an Invitrogen EVOS FL Auto 2 microscope (Thermo Fisher Scientific). Subsequent quantification of cellular fluorescence intensity was performed using ImageJ software (Version 1.53, National Institutes of Health, Bethesda, MD, USA). Alternatively, MFC-LUC cells were co-cultured with T lymphocytes at target-to-effector ratios of 1:5, 1:10, and 1:20 alongside RAW 264.7 cells in the upper chamber. After 3 days, adherent tumor cells were transferred to black 96-well plates, lysed in cell lysis buffer, and incubated with Firefly Luciferase Assay Reagent (150 µg/mL, 5 min; 11401ES60, Yeasen Biotechnology, Shanghai, P. R. China). Luminescence was quantitatively measured using an EnVision 2104 multilabel plate reader (PerkinElmer, Wellesley, MA, USA).

2.22 | In vivo bioluminescence imaging

Mice were administered D-luciferin potassium salt (150 mg/kg; 40902ES01, Yeasen Biotechnology) and anesthetized with 2.5% isoflurane. Bioluminescence signals were captured using an IVIS Lumina III imaging system (PerkinElmer, Waltham, MA, USA) and analyzed using Living Image software (Version 4.7, PerkinElmer). Bioluminescence quantification was performed by normalizing the photon flux in the defined regions of interest against areas devoid of background signals.

2.23 | Mass spectrometry

Proteins were extracted from AGS cells and analyzed using a Bruker mass spectrometer (timsTOF Pro, Bruker Cor-

poration, Ettlingen, Baden-Württemberg, Germany). The raw data were processed using MaxQuant software (1.6.14, <https://www.maxquant.org/>) with the reference proteome from the UniProt database (version 2020_01, <https://www.uniprot.org/>). Protein identification and quantification were carried out by applying a false discovery rate (FDR) threshold of 1%. Normalization was performed using the LFQ algorithm (version 1.0, <https://analyst-suite.monash-proteomics.cloud.edu.au/apps/lfq-analyst/>) for label-free quantification.

2.24 | RNA sequencing (RNA-seq)

RNA-seq was performed by Novogene (Beijing, P. R. China) on an Illumina HiSeq platform (San Diego, California, United States) with paired-end 150 bp reads. Quality control of the raw reads was conducted using FastQC (version 0.12.0, <https://github.com/s-andrews/FastQC>). Adapter trimming was performed with TrimGalore (version 0.6.1, <https://github.com/FelixKrueger/TrimGalore>). Alignment was done using HISAT2 (version 2.2.1, <https://daehwankimlab.github.io/hisat2/>) against the human genome (GRCh38), followed by transcript quantification using featureCounts (version 2.0.4) [25]. Differential expression analysis was performed using DESeq2 (version 3.19) [26] with a threshold of \log_2 fold change > 1 and FDR < 0.05 . RNA enrichment analysis was performed using clusterProfiler 3.16.1 [27].

2.25 | Exosomal miRNA profiling

For exosomal miRNA profiling, purified exosomes from the supernatants of AGS cells with or without METTL3 overexpression underwent total RNA extraction. Small RNAs were isolated using urea denaturing polyacrylamide gel electrophoresis for library preparation. miRNA sequencing was conducted using the BGISEQ-500 platform (BGI, Shenzhen, P. R. China) by Shandong Jiekai Biotechnology (Jinan, Shandong, P. R. China). Differential expression analysis was performed using DEGseq [28], and cluster enrichment analysis was conducted using the TAM tool (<http://www.cuilab.cn/tam>) to identify enriched miRNA clusters and their associated biological functions.

2.26 | miRNA target prediction

miRNA targets were predicted using the online resources miRDB (<http://mirdb.org/>), TargetScanHuman 8.0 (https://www.targetscan.org/vert_80/), and TarBase-v9.0 (<https://dianalab.e-ce.uth.gr/tarbasev9>) according to their corresponding instructions.

2.27 | Public datasets usage

We used publicly available datasets for this study. m⁶A profiling data for AGS cells were obtained from the GSE166972 dataset. The Asian Cancer Research Group (ACRG) cohort data, which includes mRNA profiles from 300 gastric tumors with follow-up information on initial metastatic sites, were obtained from GSE66229. Single-cell RNA sequencing (scRNA-seq) data from 68 samples from 20 patients, including 10 cases of peritoneal metastasis, were sourced from GSE239676. Additionally, scRNA-seq data from five pairs of primary gastric cancer samples and corresponding malignant ascites were obtained from GSE237876. All of these datasets were accessed via the Gene Expression Omnibus (<https://www.ncbi.nlm.nih.gov/geo/>).

scRNA-seq data from 14 ascites samples of gastric cancer patients were acquired from the EGAD00001006172 dataset, available at the European Genome-phenome Archive (<https://ega-archive.org>). Transcriptome data for 450 gastric cancer surgery samples from The Cancer Genome Atlas (TCGA) stomach adenocarcinoma (STAD) cohort (dataset ID: TCGA.STAD.sampleMap/HiSeqV2_PANCAN) were obtained from the Xena database (<https://xena.ucsc.edu/public>).

2.28 | m⁶A sequencing analysis

For the m⁶A sequencing analysis, the initial raw data (GSE166972) were obtained from the Gene Expression Omnibus, and then underwent quality control and preprocessing steps using FastQC (version 0.12.0, <https://www.bioinformatics.babraham.ac.uk/projects/fastqc/>) and TrimGalore (version 0.6.1, <https://github.com/FelixKrueger/TrimGalore>) to ensure data integrity. The resulting clean data were then aligned to the human reference genome GRCh38 using Bowtie2 (version v2.4.4, <https://bowtie-bio.sourceforge.net/bowtie2>) for accurate mapping. Following alignment, peak calling was performed using MACS2 (version 2.1.4, <https://github.com/macs3-project/MACS>) with the specified parameters: `-g hs -keep-dup all -bdg ext-size 100 -nomodel -q 0.05`. The mapped reads were visualized using the WashU Epigenome Browser (<https://epigenomegateway.wustl.edu/browser/>) to create genome browser tracks, and genomic features such as coding sequences (CDS), UTRs, and introns were annotated based on the Ensembl GTF file (version 74, <https://www.ensembl.org/>).

2.29 | Immune deconvolution

The association between METTL3 expression and the immune microenvironment in gastric cancer was evaluated using the transcriptome data from the TCGA STAD dataset. The Immunedeconv R package [29] was used to estimate the abundance of immune cell types based on CIBERSORT algorithm [30]. Gene expression levels, measured as fragments per kilobase of transcript per million mapped reads, were used as input with default parameters. The output, in the form of an abundance of 22 immune cell types, was used to evaluate the correlations with METTL3 mRNA levels. To account for the potential confounding effects of microsatellite instability-high (MSI-H) and Epstein-Barr virus (EBV)-positive cases, correlation analyses were also conducted after excluding these samples.

2.30 | scRNA-seq analysis

The raw scRNA-seq data matrix was processed using Cell Ranger (version 6.0, <https://github.com/10XGenomics/cellranger>) for deduplication and alignment. Batch effects were corrected with Harmony (version 1.2.0, <https://github.com/immunogenomics/harmony>). Seurat (version 4.0, <https://github.com/satijalab/seurat>) was used to filter scRNA-seq data according to the following criteria: cells with nFeature_RNA > 500, nFeature_RNA < 9,000, and percent.mt < 75 were retained. Gene expression in each cell was normalized and log transformed. Dimensionality reduction and cell clustering were performed using the t-distributed stochastic neighbor embedding (t-SNE) algorithm (resolution = 0.5). Cell types were annotated based on marker gene expression in each cluster using Annotation of cell types (ACT, version 1.0) [31], and supported by their previous analysis [32].

2.31 | Statistical analyses

All statistical analyses were performed using GraphPad Prism (version 9.5.1, GraphPad Software, San Diego, CA, USA). Unless otherwise specified, the data are presented as the results of at least three independent experiments. Differences between the two groups were evaluated using Student's *t*-test. Differences among the three groups were evaluated using one-way analysis of variance (ANOVA), and multiple comparisons were corrected using the Tukey method. Fisher's exact or chi-square tests were used to investigate the distribution of categorical variables, as

appropriate. Correlations between two continuous variables were assessed using Pearson's correlation coefficients. All statistical tests were two-tailed, with $P < 0.05$, denoting statistical significance. P values in multiple comparisons for expression levels of miRNA clusters were adjusted via the Bonferroni correction, while those in differentially expressed gene analysis for miRNA sequencing and mRNA-seq were adjusted by Benjamini-Hochberg Correction. Data are presented as mean \pm standard deviation unless otherwise indicated.

3 | RESULTS

3.1 | Exosomes from METTL3-overexpressed gastric cancer cells promoted peritoneal metastasis

In our initial clinical analysis, gastric cancer patients with elevated METTL3 levels in primary tumors had an increased risk of peritoneal metastasis compared to those with lower METTL3 expression (odds ratio = 5.146, 95% confidence interval = 1.120-24.430, $P = 0.036$), whereas no significant differences were observed in the metastatic rate to other organs (Figures 1A-B, Supplementary Figure S1, Supplementary Table S4). To validate this finding, we performed analyses on two public datasets. In the ACRG study (GSE66229, $n = 300$), METTL3 expression (detected by probe 242111_at) was significantly elevated in patients with peritoneal seeding or ascites at recurrence but not in those with metastases to the liver, bone, intra-abdominal lymph nodes, distant lymph nodes, or other sites (Supplementary Figure S2A). In a scRNA-seq dataset (GSE239676, $n = 19$), METTL3 expression was elevated in cancer cells from primary lesions with peritoneal metastases compared to those without (Supplementary Figure S2B). Taken together, these findings highlight a clinical relevance between METTL3 overexpression in primary gastric cancer lesions and peritoneal metastasis.

To test whether tumor METTL3 facilitated peritoneal metastasis by priming peritoneal PMN, we applied a widely used method to assess peritoneal metastasis [33, 34]. Briefly, METTL3 was overexpressed in MFC cells, and the expression difference between control and METTL3-overexpressed MFC cells was comparable to that observed between METTL3-low and high patients (Supplementary Figures S3A-B). The peritoneal environment of mice was preconditioned by injecting conditioned media from these cell cultures into the peritoneal cavity, followed by intraperitoneal injection of wild-type MFC cells (Figure 1C). Mice that received conditioned medium from METTL3-overexpressed MFC cells exhibited a significant increase in abdominal circumference, body weight, ascites

volume, and the number of peritoneal implanted nodules compared to the control group over time (Figures 1D-H). These findings indicate that METTL3 overexpression may promote peritoneal metastasis by priming peritoneal PMN.

To identify the specific factors involved from the conditioned medium, we isolated the exosomes or exosome-depleted supernatants from METTL3-overexpressed and control MFC cells and administered them intraperitoneally to mice as a substitute for conditioned media for preconditioning, as previously described in Figure 1C. The size and purity of the exosomes were confirmed by electron microscopy (Supplementary Figure S4). Exosomes derived from METTL3-overexpressed MFC cells (METTL3-oe-exo) substantially accelerated peritoneal metastasis progression (Figures 1I-L). In contrast, conditioned media devoid of exosomes from METTL3-overexpressed MFC cells failed to accelerate peritoneal metastasis of gastric cancer in this model (Figures 1M-P).

To further elucidate the role of exosomes in peritoneal metastasis, we established an *Smpd3* knockdown MFC cell line to reduce exosome secretion, as *Smpd3* is known to play a critical role in exosome biogenesis and secretion (Supplementary Figure S5) [35, 36]. Following *Smpd3* knockout, the conditioned medium from METTL3-overexpressed cells failed to promote peritoneal metastasis (Figures 1Q-T). Taken together, these results indicate that METTL3 overexpression may promote peritoneal metastasis via exosome secretion.

3.2 | METTL3 enhanced exosome biogenesis in gastric cancer by upregulating RAB27A expression

To explore the role of METTL3 in exosome secretion and function, we established human gastric cancer cell lines with METTL3 overexpression in AGS cells and METTL3 knockdown in MKN-45 selected based on their respective low and high baseline METTL3 expression levels (Figure 2A). METTL3-overexpressed cells exhibited increased exosome production, whereas METTL3 knockdown reduced exosome production (Figures 2B-C). Mass spectrometry analysis of lysates from METTL3-overexpressed and control AGS cells identified RAB27A as one of the most significantly upregulated proteins in METTL3-overexpressed AGS cell lysates (Figure 2D). Given its well-established role in exosome biogenesis [37, 38], RAB27A was selected for further investigation. Western blotting demonstrated that RAB27A protein levels were significantly elevated in METTL3-overexpressed cells and downregulated in METTL3-knockdown cells compared to control cells, supporting the regulatory link between METTL3 and RAB27A (Figure 2E).

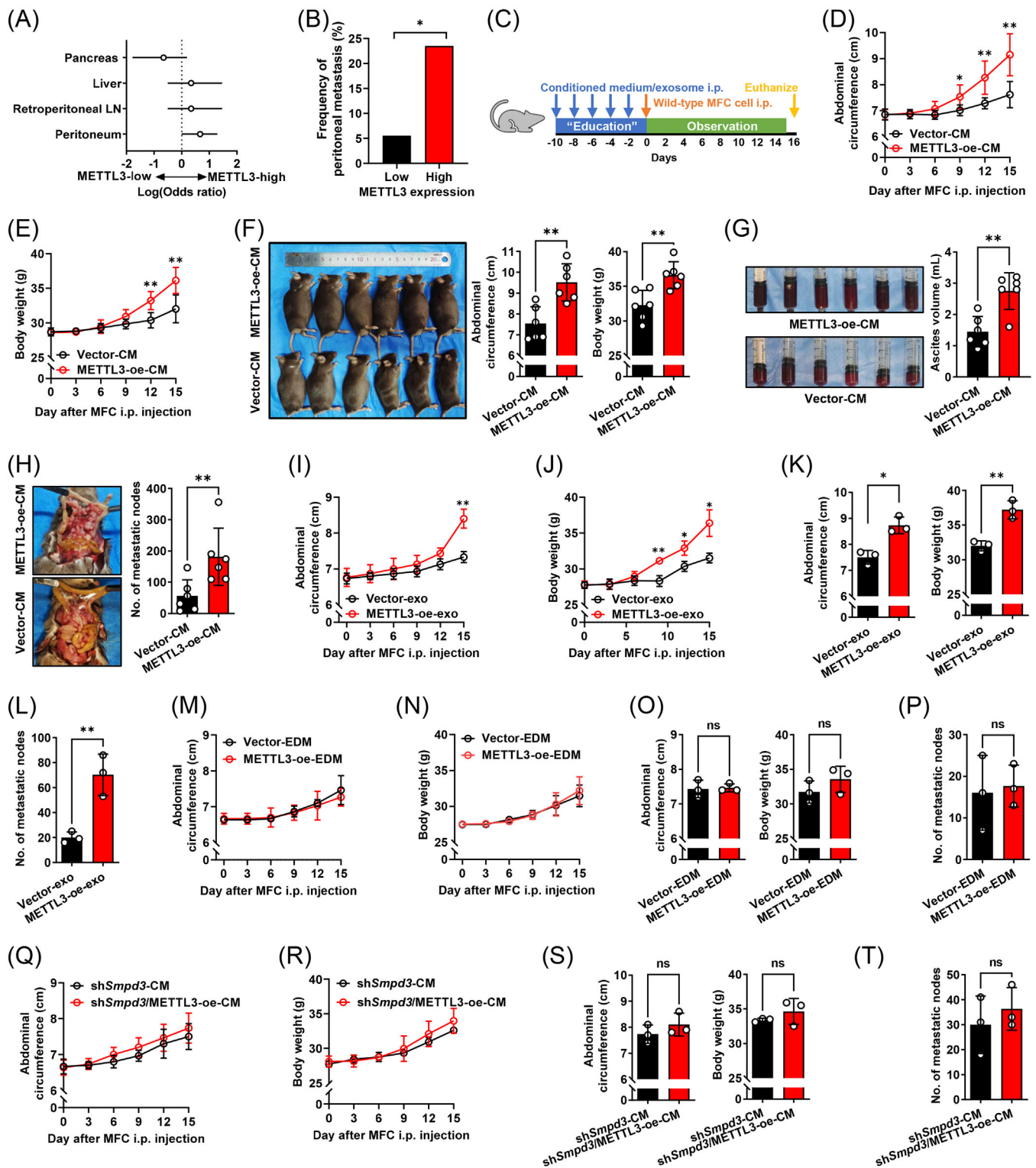


FIGURE 1 Impact of exosomes derived from METTL3-overexpressed GC cells on peritoneal metastasis. (A) Association between METTL3 expression and metastasis rates on various organ in GC patients. (B) Incidence of peritoneal metastasis in METTL3-high and -low GC patients. (C) Schematic diagram of the establishment of the peritoneum "education" model. The peritoneal environment was preconditioned by intraperitoneal (i.p.) injections of conditioned media (CM) or exosomes (exo) on days -10, -8, -6, -4, and -2, followed by i.p. injections of wild-type MFC cells. Models were observed for 15 days and euthanized on day 16. (D-E) The changes of abdominal circumferences (D) and body weights (E) of mice treated with CM culturing METTL3-overexpressed (METTL3-oe-CM) and control (Vector-CM) MFC cells since wild-type MFC cells injection. Mouse per group, $n = 6$. Asterisks indicate statistically significant differences at the corresponding time points. (F-H) Assessment of peritoneal "education" models, showing appearance (F), ascites volume (G), and peritoneal implants (H) on day 16, with

In addition, *RAB27A* knockdown in METTL3-overexpressed cell lines reversed the increase in exosome secretion (Figures 2F-G). By contrast, *RAB27A* overexpression in METTL3-knockdown cell lines rectified diminished exosome secretion (Figures 2H-I). These findings suggest that METTL3 may facilitate exosome secretion by modulating *RAB27A* expression.

3.3 | METTL3 facilitated *RAB27A* mRNA translation via A502 m⁶A modification and subsequent recognition by YTHDF1

Since METTL3 is a well-known “m⁶A writer”, we subsequently focused on its m⁶A modification functions. Mutation of the methyltransferase domain of METTL3 abolished its ability to enhance *RAB27A* expression and exosome secretion in AGS cells, indicating that METTL3 regulation of *RAB27A* may be potentially m⁶A-dependent (Figures 2J-K).

RNA immunoprecipitation experiments demonstrated that METTL3 increased the m⁶A modification level of *RAB27A* without affecting its mRNA levels or stability (Figures 2L-N). Inhibiting ribosomal function with anisomycin proportionally decreased *RAB27A* levels in both METTL3-overexpressed and control cells, implying that the observed increase in *RAB27A* protein levels in METTL3-overexpressed cells is not due to reduced protein degradation (Figure 2O). In addition, we isolated RNA fractions by polysome profiling and found that *RAB27A* mRNA levels in the translation-active polysomes were significantly higher in METTL3-overexpressed cells than in the control cells (Figure 2P).

Analysis of m⁶A sequencing data revealed several specific modification sites within the coding sequence region of the final exon of *RAB27A* mRNA in AGS cells, notably at the nucleotide positions 502, 536, and 569 (Figure 2Q, Supplementary Figure S6). Among these, the mutation c.502A>C significantly suppressed *RAB27A* expression and inhibited m⁶A modification (Figures 2R-S).

YTHDF1 has been reported to be the primary m⁶A “reader” in regulating m⁶A-dependent translation. Using an anti-YTHDF1 antibody for RIP, we unequivocally demonstrated its binding to *RAB27A* mRNA in both wild-type AGS and MKN-45 cells (Figure 2T). This specific binding was confirmed by reverse RNA pull-down using *RAB27A* mRNA probes (Figure 2U). Notably, in the METTL3-overexpressed cell line, YTHDF1 exhibited an increased affinity for *RAB27A* mRNA, whereas in the METTL3-knockdown cell line, the proportion of *RAB27A* mRNA bound to YTHDF1 was reduced (Figure 2V). Compared to cells transfected with wild-type *RAB27A*, cells transfected with mutant *RAB27A*-502C showed a decreased ratio of *RAB27A* mRNA bound to YTHDF1 (Figure 2W). At the protein level, YTHDF1 overexpression alone did not increase *RAB27A* translation. However, in the presence of a plasmid containing wild-type *RAB27A*, YTHDF1 significantly enhanced *RAB27A* expression. This effect was not observed in cells overexpressing *RAB27A*-502C (Figure 2X). *YTHDF1* knockdown also counteracted the *RAB27A* upregulation by METTL3 (Figure 2Y). These data suggest that METTL3 orchestrates *RAB27A* translation through m⁶A modification at the 502 site of *RAB27A* mRNA, with YTHDF1 serving as a crucial reader in this intricate process.

3.4 | Exosomes from METTL3-overexpressed cells induced an immunosuppressive PMN in the peritoneal cavity

Early tumor metastasis was evaluated on day 6 (Figure 3A). After euthanizing the mice, comprehensive analyses, including immunofluorescence, flow cytometry, and qPCR, collectively showed a higher number of peritoneal metastatic cells in METTL3-oe-exo treated mice compared to those treated with control exosomes (Figures 3B-D).

To elucidate the mechanism underlying exosome-mediated tumor cell metastasis, we established an

images on the left and quantification on the right. Mouse per group, $n = 6$. (I-L) Changes in abdominal circumferences (I) and body weights (J) in mice treated with exosomes from METTL3-oe or control MFC cells, starting from injection with MFC cells, as well as comparison of these parameters (K), and metastatic nodule numbers (L) on day 16. Mouse per group, $n = 3$. Asterisks indicate statistically significant differences at the corresponding time points in (I-J). (M-P) Abdominal circumferences (M) and body weights (N) in mice treated with exosome-depleted media (EDM) from METTL3-oe or control MFC cells, starting from injection with MFC cells, as well as comparison of these parameters (O), and metastatic nodule counts on day 16 (P). Mouse per group, $n = 3$. (Q-T) Changes of abdominal circumferences (Q) and body weights (R) in mice treated with CM from control or METTL3-oe MFC cells with *Smpd3*-knockdown (sh*Smpd3*-CM, sh*Smpd3*/METTL3-oe-CM), starting from injection with MFC cells, as well as comparison of these parameters (S), and metastatic nodule counts at day 16 (T). Mouse per group, $n = 3$. Data are presented as mean \pm standard deviation. ns, not significant; * $P < 0.05$; ** $P < 0.01$; *** $P < 0.001$. Abbreviations: CM, conditioned media; EDM, exosome-depleted media; exo, exosomes; GC, gastric cancer; i.p., intraperitoneal; LN, lymph node; METTL3-oe, METTL3-overexpressed; sh*Smpd3*, *Smpd3*-knockdown; *Smpd3*, sphingomyelin phosphodiesterase 3.

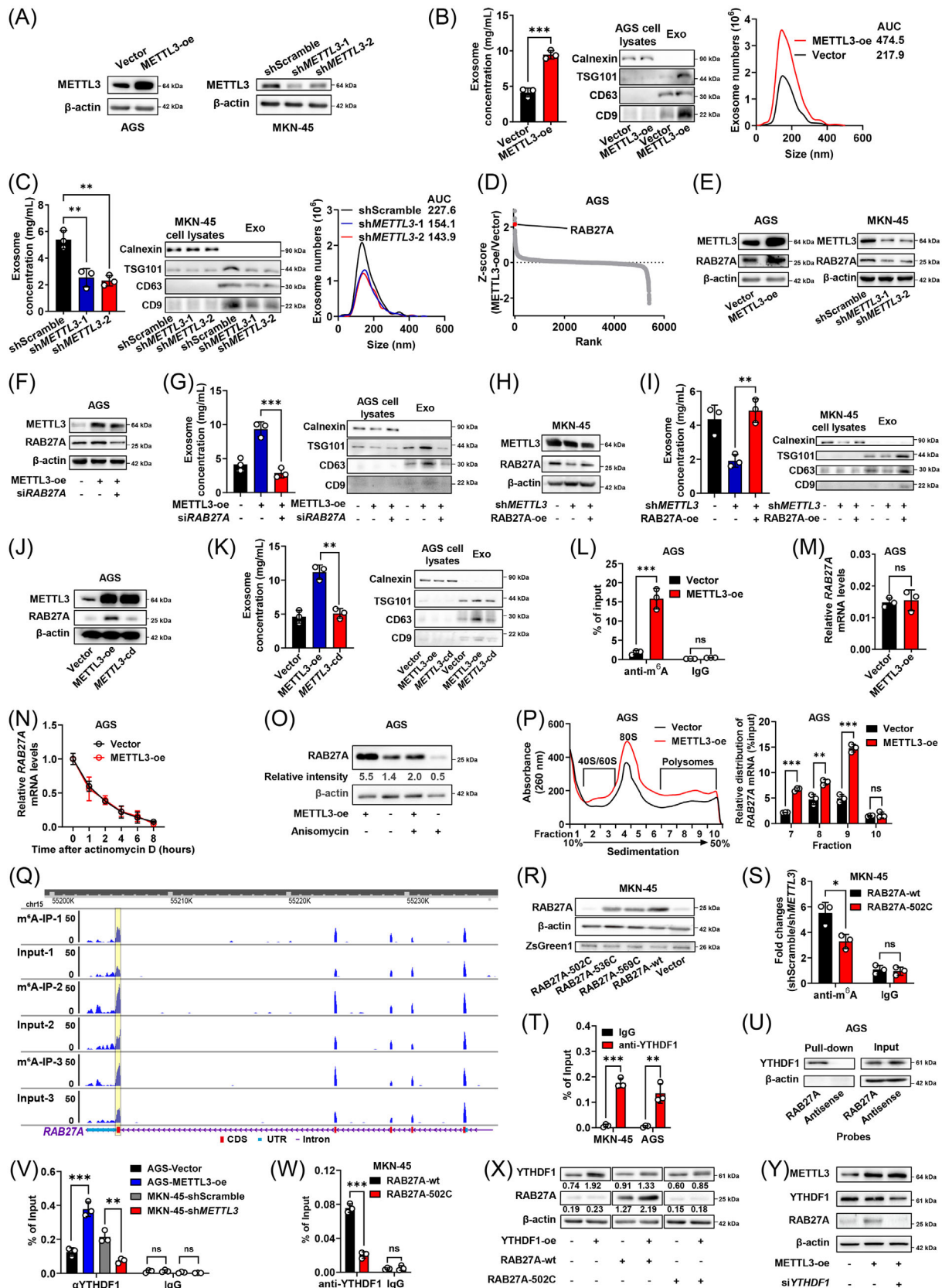


FIGURE 2 METTL3 facilitated exosome production via RAB27A N6-methyladenosine (m⁶A) modification and YTHDF1 recognition. (A) Western blotting results of METTL3 levels in AGS cells transfected with METTL3-overexpressed (METTL3-oe) plasmid, MKN-45 cells transfected with shRNA against *METTL3* (shMETTL3), and respective controls (vector and shScramble). (B-C) Exosome release quantification from AGS cells with METTL3-oe (B), MKN-45 cells with shMETTL3 (C), and their corresponding control cells, using

experimental tumor-peritoneal adhesion model (Figure 3E). METTL3-oe-exo did not directly increase the number of adherent MFC cells (Figure 3F). However, when PLC were introduced, MFC cell adherence was reduced significantly. Intriguingly, the addition of PLC from METTL3-oe-exo treated mice reversed this effect, indicating that METTL3-oe-exo influenced tumor cell-peritoneum interactions by modulating peritoneal cavity cells rather than tumor cells (Figure 3G). This phenomenon was validated *in vivo* using adoptive cell transfer experiments, in which PLC from METTL3-oe-exo treated mice promoted peritoneal metastasis in recipient mice (Figures 3H-M). Additionally, while *in vitro* treatment with METTL3-oe-exo enhanced tumor cell proliferation and invasive ability, it did not reduce the tumor-killing efficacy of T lymphocytes (Supplementary Figure S7).

Further characterization of METTL3-oe-exo-induced PMN was performed using flow cytometry analysis of peritoneal immune cells (Figure 3N). In PLC from METTL3-

oe-exo-treated mice, the ratio of macrophages increased, whereas the ratio of T lymphocytes decreased compared to those in control exosome-treated mice. In addition, the CD8⁺/CD3⁺ T cell ratio was notably reduced (Figure 3O). Conversely, intraperitoneal injection of METTL3-oe-exo did not influence the proportion of immune cells in the peripheral blood and spleen (Supplementary Figure S8).

We used several datasets to validate these *in vivo* findings. In the TCGA STAD cohort, METTL3 expression was positively correlated with M0, M1, and M2 macrophages while negatively correlated with CD8⁺ T lymphocytes, regardless of the inclusion or exclusion of MSI-H and EBV-positive tumors (Figure 3P and Supplementary Figure S9). In the scRNA-seq dataset (GSE239676), tumor METTL3 levels in primary tumor lesions were positively correlated with tumor-associated macrophages and negatively correlated with inflammatory macrophages, CD8⁺ T cells, and CD8⁺/CD4⁺ T cell ratio in ascites (Supplementary Figures S10A-C). In another scRNA-seq dataset comprising evalu-

bicinchoninic acid assay (left, $n = 3$ per group), Western blotting (middle), and nanoparticle tracking analysis (right). In the Western blotting analysis, cell lysates were used as controls to confirm the specificity of exosome-associated protein detection. (D) Comparative proteomic profiling of METTL3-oe vs. control AGS cell lysates via mass spectrometry. Normalized Z-scores of fold changes of each protein levels are shown, with the red point highlights RAB27A. (E) Western blotting result showing RAB27A protein levels in cells with different METTL3 expression levels. (F-G) Expression levels of METTL3 and RAB27A in AGS cells of control, METTL3-oe, and METTL3-oe with *RAB27A* knockdown (si*RAB27A*) (F), and quantification of their exosome releases (G) using bicinchoninic acid assay (left, $n = 3$ per group) and Western blotting (right). (H-I) Expression levels of METTL3 and RAB27A in MKN-45 cells of control, sh*METTL3*, and sh*METTL3* with *RAB27A*-overexpressed (*RAB27A*-oe) (H), and quantification of their exosome releases (I) using bicinchoninic acid assay (left, $n = 3$ per group) and Western blotting (right). (J-K) *RAB27A* expression levels in AGS cells with METTL3-oe or a catalytically dead *METTL3* mutant (*METTL3*-cd) (J), and exosome quantification with bicinchoninic acid assay (left, $n = 3$ per group) and Western blotting (right) (K). (L-M) m⁶A (L) and mRNA (M) levels of *RAB27A* in METTL3-oe vs. control AGS cells. IgG was used as a negative control in (L). $n = 3$ per group. (N) *RAB27A* mRNA stability in control and METTL3-oe AGS cells. Actinomycin D was used to inhibit transcription, and relative mRNA levels (normalized to baseline at 0 hour) were measured by quantitative PCR at different time points, $n = 3$ per group. (O) *RAB27A* protein degradation in METTL3-oe and control AGS cells. Anisomycin was used to inhibit translation, and protein levels were measured by Western blotting. The numbers below each lane indicate the relative intensity of *RAB27A*, normalized to β -actin. (P) Polysome profiling of METTL3-oe and control cells (left) and relative *RAB27A* mRNA enrichment in polysome fractions 7 to 10 by quantitative PCR (right). $n = 3$ per group. (Q) Mapping of m⁶A modifications within the *RAB27A* locus using m⁶A sequencing data in AGS cells, with the significantly enriched m⁶A modification region highlighted in yellow. Data of GSE1166972 were preprocessed using FastQC and Trim Galore for quality control and aligned to the GRCh38 reference genome using Bowtie2. Peak calling was performed with MACS2, and the results were visualized using the WashU Epigenome Browser with annotations based on the Ensembl GTF file. The “input” refers to the total RNA samples used for m⁶A enrichment analysis, while “m⁶A-IP” indicates the RNA samples processed through m⁶A-immunoprecipitation. (R) *RAB27A* levels in MKN-45 cells transfected with a *RAB27A*-expressing plasmid or mutants. ZsGreen1 was probed to evaluate transfection efficiency. (S) Fold changes in *RAB27A* m⁶A levels between shScramble and sh*METTL3* MKN-45 cells expressing wild-type (*RAB27A*-wt) or c.502A>C mutant (*RAB27A*-502C) *RAB27A*. $n = 3$ per group. (T-U) Results of RNA-immunoprecipitation assay in AGS and MKN-45 cells (T) and reverse RNA-pull-down in AGS cells (U) to validate YTHDF1 binding to *RAB27A* mRNA. (V-W) YTHDF1 interaction with *RAB27A* mRNA in AGS and MKN-45 cells with varying METTL3 expression (V) and MKN-45 cells with wild-type or mutated *RAB27A* (W). $n = 3$ per group. (X) *RAB27A* and YTHDF1 expression in AGS cells with differing YTHDF1 expression and *RAB27A* mutations. Relative protein intensities relative to β -actin, as quantified by ImageJ, are shown below each band. (Y) Western blotting analysis of METTL3, YTHDF1, and *RAB27A* protein expression in AGS cells with control vector, METTL3-oe, and METTL3-oe and *YTHDF1* knockdown (si*YTHDF1*). Data are presented as mean \pm standard deviation. ns, not significant; * $P < 0.05$; ** $P < 0.01$; *** $P < 0.001$. Abbreviations: AUC, area under the curve; m⁶A, N⁶-methyladenosine; METTL3, Methyltransferase-like 3; *METTL3*-cd, catalytically dead METTL3; METTL3-oe, METTL3-overexpressed; *RAB27A*, ras-related protein Rab-27A; *RAB27A*-wt, wild-type *RAB27A*; *RAB27A*-502C, *RAB27A* c.502A>C mutant; *RAB27A*-oe, *RAB27A*-overexpressed; sh*METTL3*, shRNA against *METTL3*; shScramble, scramble shRNA; si*RAB27A*, *RAB27A* knockdown; si*YTHDF1*, *YTHDF1* knockdown; YTHDF1, YTH N⁶-methyladenosine RNA binding protein 1; YTHDF1-oe, YTHDF1-overexpressed.

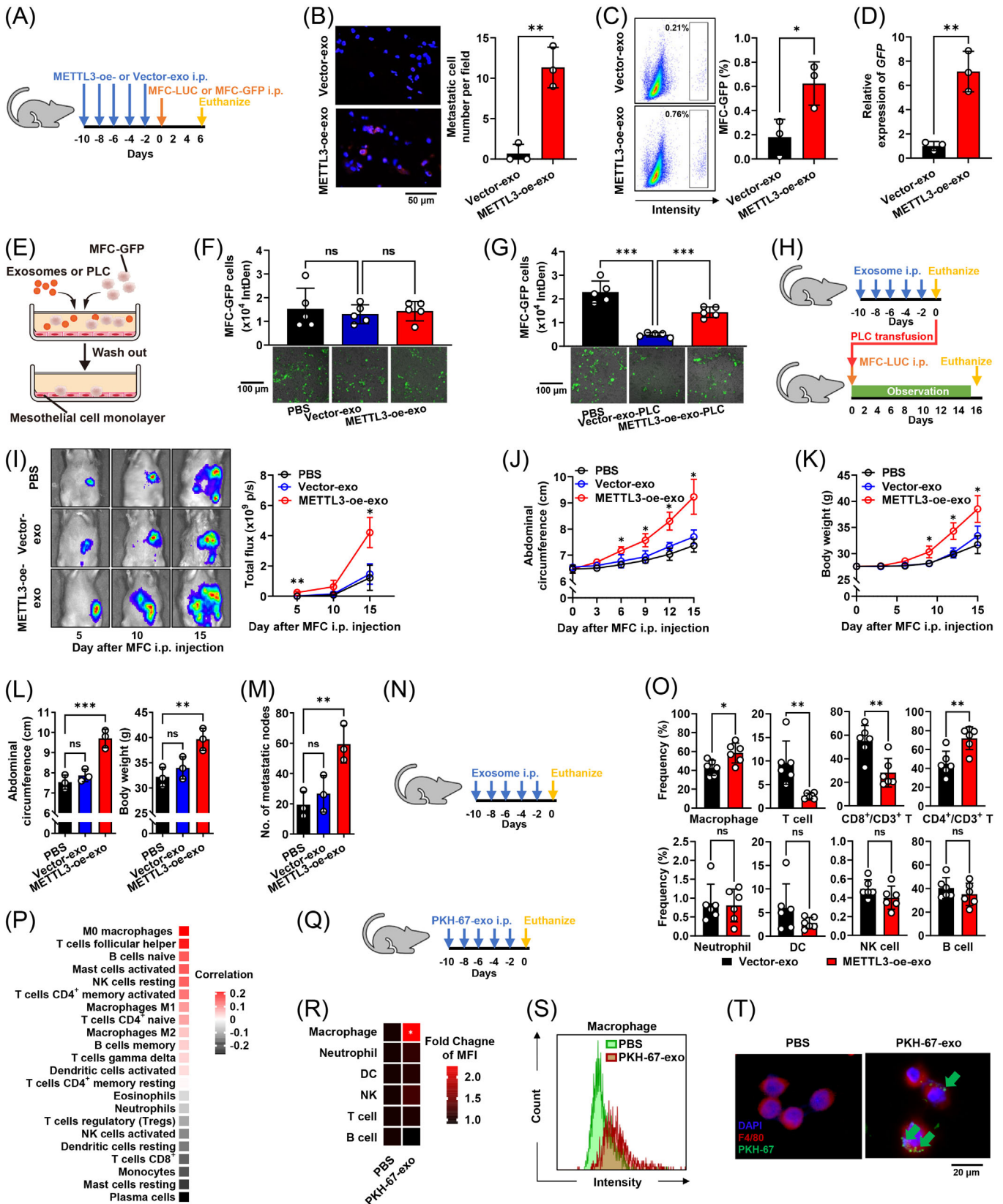


FIGURE 3 Exosome from METTL3-overexpressed induced immunosuppressive PMN in the peritoneum. (A) Schematic diagram illustrating the experimental workflow for studying early phase of peritoneal metastasis under exosome (exo)-mediated reprogramming. The peritoneal environment was preconditioned by intraperitoneal (i.p.) injections of exo from METTL3-overexpressed (METTL3-oe-exo) or control (vector-exo) MFC cells on days -10, -8, -6, -4, and -2, followed by i.p. injections of wild-type MFC cells expressing luciferase

able ascites lymphocyte populations (EGAD00001006172), tumor METTL3 was also found to be negatively correlated with activated T cells, activated CD8⁺ T cells, and activated CD8⁺/CD4⁺ T cell ratio in ascites (Supplementary Figure S11). Additionally, RNA-seq of paired primary tumors and ascites in the GSE237876 dataset showed a similar trend, with tumor METTL3 expression positively correlating with ascites macrophage ratios and negatively correlating with CD8⁺ T cell ratios (Supplementary Figure S12). Furthermore, flow cytometry analysis of the ascites cells from 12 gastric cancer patients revealed that METTL3-high patients exhibited higher macrophage frequencies in ascites (Supplementary Figure S13).

3.5 | Exosome-induced immunosuppressive PMN was primarily driven by peritoneal macrophages

To delineate the specific cell targets affected by METTL3-oe-exo, we labeled exosomes with PKH-67 and intraperitoneally injected them into mice (Figure 3Q). Subsequent flow cytometry analysis of PLC demonstrated that macrophages took up a substantial quantity of exosomes, whereas uptake by T lymphocytes was neg-

ligible (Figures 3R-S). Immunofluorescence confirmed macrophage intake of METTL3-oe-exo (Figure 3T), shedding light on the preferential interaction between METTL3-oe-exo and macrophages in shaping the isPMN.

Upon identifying macrophages as the primary regulatory targets of exosomes, we investigated specific alterations in macrophage behavior in response to METTL3-oe-exo treatment. METTL3-oe-exo promoted macrophage proliferation, as determined by cell counting, but did not alter the expression of the classical M1 and M2 markers, CD80 and CD206, as assessed via flow cytometry (Figures 4A-B). Instead, RNA-seq analysis revealed that immune response-related cytokine production was enriched in METTL3-oe-exo-treated macrophages (Figure 4C). In particular, we observed upregulation of immunosuppressive IL-10 family members, *Il-10* and *Il-19*, in METTL3-oe-exo-treated RAW 264.7 macrophages (Figure 4D). qPCR and ELISA validated these findings. *In vitro*, METTL3-oe-exo increased mRNA levels of *Il-10* and *Tgf-β* while reducing those of *Il-1*, *Il-6*, *Il-12*, and *Tnf*, and the changes in protein levels of IL-1, IL-6, IL-10, and TGF-β were also validated (Figures 4E-F). These cytokine changes were confirmed in peritoneal lavage fluid of METTL3-oe-exo-treated mice in the previously described model (Figures 1H-J), as shown in Figure 4G.

(MFC-LUC) or green fluorescent protein (MFC-GFP) on day 0. Then mice were euthanized on day 6 to evaluate tumor seeding. (B-D) Early detection of micro-metastatic seeding on day 6 using immunofluorescence with anti-luciferase antibody (B), flow cytometry targeting GFP (C), and quantitative PCR with GFP-specific primers (D). Samples were collected from the peritoneum of mice injected with METTL3-oe-exo or vector-exo followed by injection of MFC-LUC (B) and MFC-GFP (C-D) cells. Mouse per group, $n = 3$. (E) Schematic diagram showing *in vitro* tumor-peritoneum adhesion assay. A monolayer of 615 mouse mesothelial cells was established, and MFC-GFP cells were added to evaluate their adhesion to the peritoneal lining under conditions with or without exosomes or peritoneal lavage cells (PLC). (F-G) Quantifications of adhered MFC-GFP cells after treatment with METTL3-oe-exo or vector-exo (F) and with PLC derived from mice treated with METTL3-oe-exo or vector-exo (G), with the representative images shown below and quantifications by fluorescence density above. $n = 5$ per group. (H) Schematic representation of PLC transfer. Donor mice were treated with exosomes for ten days and then euthanized to obtain PLC. The PLC was then co-transferred with MFC-LUC to the recipient mice, and peritoneal metastasis was assessed. (I-M) Changes of the tumor luciferase signal intensity (I), abdominal circumferences (J), and body weights (K) in the peritoneal metastasis models established with PLC transfusion from the mice educated with METTL3-oe-exo or vector-exo, followed by MFC-LUC *i.p.* injection. Asterisks indicate significant differences between the METTL3-oe-exo group and the phosphate buffered saline (PBS) group at corresponding timepoints in (I-K). Additionally, the comparison of abdominal circumferences and body weights (L), and the metastatic nodule numbers (M) at day 16 were analyzed. Mouse per group, $n = 3$. (N) Schematic representation of PLC population analysis. Exosomes were *i.p.* injected into mice at days -10, -8, -6, -4, and -2 and the mice were euthanized for PLC population analysis at day 0. (O) Frequencies of different cell populations within the total cell count in mice pretreated with vector-exo or METTL3-oe-exo. Mouse per group, $n = 6$. (P) Correlation between METTL3 expression and the immune landscape in gastric cancer patients, including microsatellite instability-high and Epstein-Barr virus-positive cases, using TCGA STAD dataset. (Q) Schematic representation of the exosome tracing experiment. PKH-67-labeled exosomes were *i.p.* injected into mice at days -10, -8, -6, -4, and -2 and the mice were euthanized at day 0. (R) Heatmap illustrating the uptake fold changes of PKH-67-labeled exosomes by various peritoneal cell types. The fold changes of mean fluorescence intensity (MFI) between cells from mice treated with PKH-67-labeled exosomes and those treated with PBS are shown. Mouse per group, $n = 3$. (S-T) PKH-67-labeled exosome uptake by macrophages was detected by flow cytometry (S) and fluorescence microscopy (T). Red indicates anti-F4/80 antibody and green indicates PKH-67. Green arrows indicate the exosomes that have been taken up by macrophages. Data are presented as mean \pm standard deviation. ns, not significant; * $P < 0.05$; ** $P < 0.01$; *** $P < 0.001$. Abbreviations: DC, dendritic cell; exo, exosome; IntDen, integrated density; METTL3-oe, METTL3-overexpressed; MFC-LUC, MFC cells expressing luciferase; MFC-GFP, MFC cells expressing green fluorescent protein; MFI, mean fluorescence intensity; NK, natural killer; PBS, phosphate buffered saline; PLC, peritoneal lavage cells; PMN, pre-metastatic niche; STAD, stomach adenocarcinoma; TCGA, The Cancer Genome Atlas.

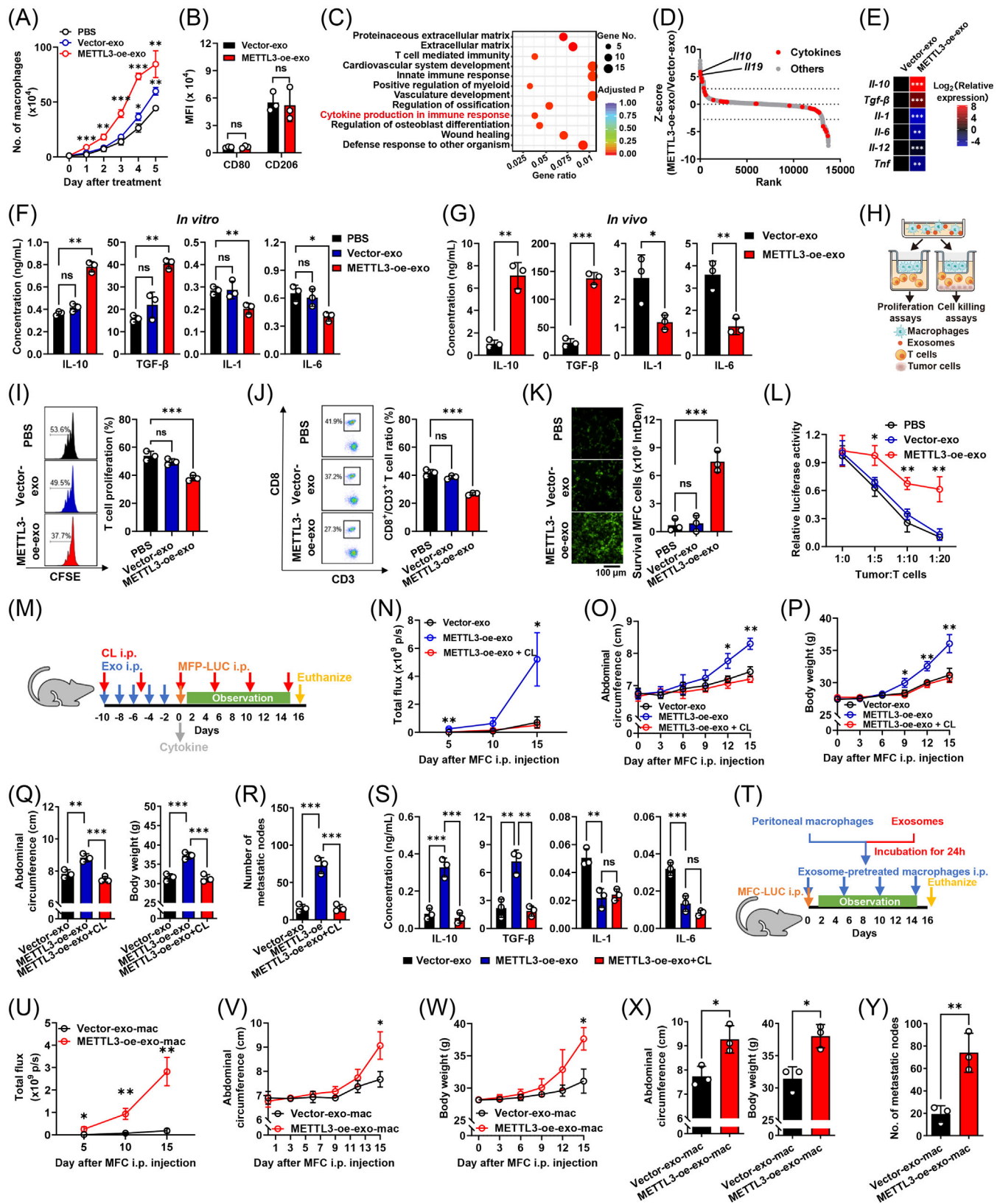


FIGURE 4 Exosomes from METTL3-overexpressed cells reprogrammed peritoneal macrophages to establish an immunosuppressive PMN. (A-B) Macrophage proliferation (A) and surface marker expression (B) when cocultured RAW 264.7 cells with exosomes from control (vector-exo) and METTL3-overexpressed (METTL3-oe-exo) MFC cells. $n = 3$ per group. Asterisks indicate significant differences between the METTL3-oe-exo or vector-exo groups and the PBS control at corresponding timepoints in (A). (C-D) Gene set enrichment analysis of

In clinical patients, IL-10 and TGF- β were elevated in malignant ascites compared to cirrhotic ascites, whereas IL-6 was not significantly different (Supplementary Figure S14). Besides, in the dataset GSE239676, we identified a negative correlation between tumor *METTL3* mRNA levels and ascites macrophage *IL-1B* and *TNF*, as well as a positive correlation between tumor *METTL3* mRNA levels and ascites macrophage *TGF-B1* (Supplementary Figure S15).

Using a Transwell co-culture model, we demonstrated that *METTL3*-oe-exo-treated macrophages inhibited T-lymphocyte proliferation, decreased CD8⁺/CD3⁺ T lymphocyte ratios, and suppressed T lymphocyte cytotoxicity against MFC cells (Figures 4H-L). Conversely, direct exposure of T lymphocytes to exosomes caused no significant changes (Supplementary Figure S16).

To determine the role of macrophages in peritoneal PMN, we depleted macrophages using clodronate liposomes during exosome “education” (Figure 4M). We observed a reversal of the pro-metastatic effects induced by *METTL3*-oe-exo in the peritoneal cavity (Figures 4N-R). Macrophage depletion prior to tumor implantation also reversed the changes in IL-10 and TGF- β levels in PMN (Figure 4S). Additionally, a macrophage-tumor co-transplantation model revealed that the transfer of in vitro *METTL3*-oe-exo pretreated macrophages promoted MFC cell peritoneal metastasis (Figure 4T-Y). These findings underscore the pivotal role of macrophages in the context of exosome-induced peritoneal PMN.

3.6 | Exosomal miR-17-92 drove macrophage polarization in PMN

Through miRNA sequencing, we identified significant enrichment of upregulated miRNAs in *METTL3*-oe-exo within the miR-17-92 cluster, indicating their critical roles (Figure 5A). miRNAs within this cluster were highly conserved, with nearly identical seed sequences between mice and humans (Supplementary Figure S17). miR-17-92 cluster expression was elevated in both *METTL3*-overexpressed AGS and MFC cells and the exosomes they produced; however, this increase was not significant when *METTL3*-cd was introduced (Figure 5B and Supplementary Figure S18A). Furthermore, exosomal miR-17-92 levels were also elevated in malignant ascites from gastric cancer patients compared to those in benign ascites (Supplementary Figure S18B). Importantly, introducing miR-17-92 into macrophages resulted in identical shifts in cytokine profiles and the ability to inhibit T cell proliferation and cytotoxicity against MFC cells (Figures 5C-I). These effects mirrored the effects of *METTL3*-oe-exo in macrophages regarding cytokine profiles, T cell proliferation, and cytotoxicity against tumors (Figures 4E-F and H-L).

Moreover, we generated exosomes enriched with miR-17-92 by overexpressing *mir17hg* in MFC cells and collecting exosomes from the supernatant of these cells. Analysis revealed that these exosomes exhibited increased levels of miR-17-92 (Figure 5J). These exosomes induced an imbal-

differentially expressed genes (C) and gene expression fold changes (D) in macrophages treated with *METTL3*-oe-exo vs. vector-exo. (E-F) Cytokine expression in RAW 264.7 cells treated with *METTL3*-oe-exo vs. vector-exo with quantitative PCR (E) and enzyme-linked immunosorbent assay (F) in vitro. $n = 3$ per group. (G) Ascites cytokine levels in peritoneal metastasis models administered with *METTL3*-oe-exo vs. vector-exo. $n = 3$ per group. (H) Schematic of the Transwell co-culture system. RAW 264.7 cells pre-treated with exosomes were placed in the upper chamber, and mouse T cells were cultured in the lower chamber, either alone or in the presence of MFC cells, for assessment of T cell proliferation and tumor cell-killing activity. (I-J) Analysis of T cell proliferation by CFSE fluorescence intensity (I) and CD8⁺/CD3⁺ T cell ratio detected by flow cytometry (J) in response to phosphate buffered saline (PBS) or exosome-treated macrophages. $n = 3$ per group. (K-L) Cytotoxicity evaluation using fluorescence density (K) and luciferase activity (L) in surviving MFC cells. $n = 3$ per group. Asterisks indicate significant differences between *METTL3*-oe-exo and PBS groups at corresponding tumor-to-T-cell ratios in (L). (M) Macrophage depletion strategy using clodronate liposomes (CL) or control liposomes at five-day intervals from the start of education to euthanasia. (N-R) Changes in MFC-LUC cell luciferase signal intensity (N), abdominal circumferences (O), and body weights (P) in the gastric cancer peritoneal metastasis model with exosome “education” and macrophage depletion, comparison at day 16 (Q) and metastatic nodule numbers (R). Mouse per group, $n = 3$. Asterisks indicate significant differences between *METTL3*-oe-exo and vector-exo groups at the corresponding timepoints in (N-P). (S) Comparison of cytokine profiles in peritoneal PMN under exosome education and macrophage depletion. Mouse per group, $n = 3$. (T) Schematic of the macrophage transfer experiment. Macrophages were collected from mouse peritoneum and pretreated with different exosomes for 24 h. Subsequently, the macrophages were administered intraperitoneally every 5 days for a total of four times to the peritoneal metastasis models. (U-Y) Changes in tumor luciferase signal intensity (U), abdominal circumferences (V), and body weights (W) in MFC peritoneal metastasis model with vs. without macrophage adoptive transfusion, comparison at day 16 (X) and metastatic nodule numbers (Y). Mouse per group, $n = 3$. Asterisks indicate statistically significant differences at the corresponding time points in (U-W). Data are shown as mean \pm SD. ns, not significant; * $P < 0.05$; ** $P < 0.01$; *** $P < 0.001$. CL, clodronate liposomes; CFSE, carboxyfluorescein succinimidyl ester; ELISA, enzyme-linked immunosorbent assay; IntDen, integrated density; mac, macrophages; *METTL3*-oe, *METTL3*-overexpressed; PBS, phosphate buffered saline; qPCR, quantitative polymerase chain reaction; PMN, pre-metastatic niche; TGF- β , transforming growth factor- β ; TNF, tumor necrosis factor.

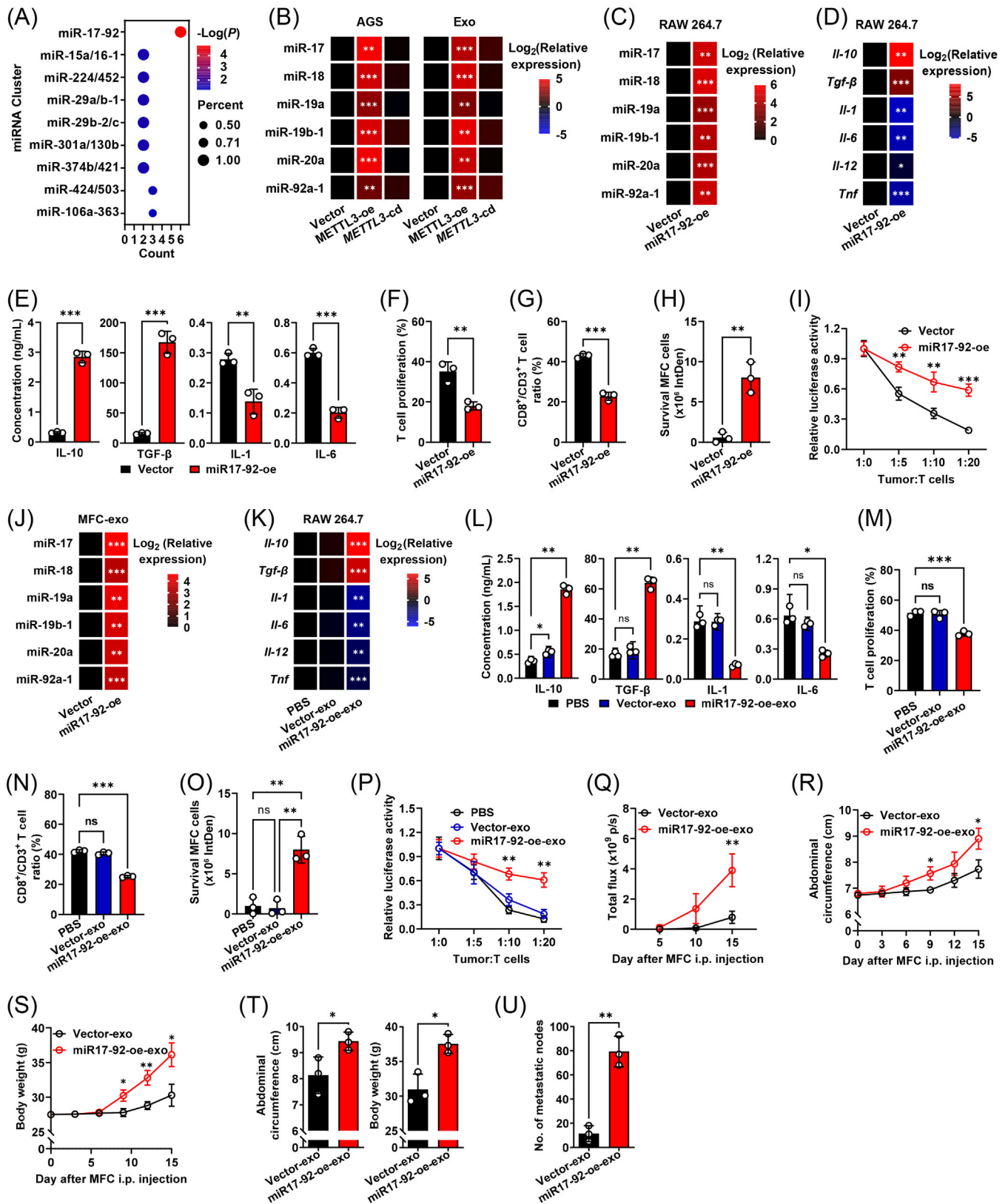


FIGURE 5 Exo-miR-17-92 cluster drove macrophage polarization to the pro-PMN subtype. (A) miRNA cluster enrichment of differentially expressed exosomal miRNAs from METTL3-overexpressed (METTL3-oe) and control (vector) AGS cells via miRNA sequencing. “Percent” refers to the percentage of differentially expressed miRNAs within the miRNA cluster, while “Count” represents the number of differentially expressed miRNAs. (B) Quantitative PCR (qPCR) results of miR-17-92 cluster expression in AGS cells with METTL3-oe or with catalytically dead METTL3 mutation (METTL3-cd), and their exosomes (exo). *n* = 3 per group. (C) qPCR results of miR-17-92 cluster

ance in macrophage cytokine secretion, which hindered T-cell proliferation and cytotoxicity against MFC cells and facilitated peritoneal metastasis (Figures 5K-U).

3.7 | Exosomal miR-17-92 cluster modulated macrophages via SRC proto-oncogene, non-receptor tyrosine kinase (SRC) activation

To identify the precise targets and pathways through which miR-17-92 from METTL3-oe-exo regulates macrophages, we conducted an intersection analysis between the down-regulated genes identified by RNA-seq in macrophages treated with METTL3-oe-exo and the predicted target genes of the miR-17-92 cluster. This analysis identified 14 overlapping genes, with *Srcin1* ranking first as the target of the two members (miR-17 and miR-20a) (Figure 6A). The miR-17/miR-20a-*SRCIN1* interaction was also predicted based on analysis with the TargetScanHuman tool and the TarBase database (Supplementary Figures S19A-B). In macrophages overexpressing miR-17-92, we observed reduced SRCIN1 protein expression, increased phosphorylation at the activation site (Y424, corresponding to the sequence of P05480-1 in UniProt) of SRC, and decreased phosphorylation at the inhibition site (Y535) of SRC (Figure 6B). Luciferase reporter assays confirmed that both miR-17 and miR-20a suppressed SRCIN1 expression, whereas their inhibitors promoted SRCIN1 expression. These miRNA mimics or miRNA inhibitors did not significantly affect the expression of the mutant plasmids (Figure 6C). Treatment with an SRC inhibitor, SRC inhibitor-1, effectively reversed the anti-inflammatory phenotype induced by the miR-17-92 cluster in macrophages

and promoted T-cell proliferation and cytotoxicity against MFC cells (Figures 6D-I). In summary, the miR-17-92 cluster from METTL3-oe-exo triggers a pro-PMN phenotype in macrophages through activation of the SRC pathway, ultimately promoting gastric cancer peritoneal metastasis.

4 | DISCUSSION

Peritoneal metastasis commonly occurs with gastric cancer and is characterized by poor prognosis and a lack of effective interventions. Comprehensive elucidation of the underlying molecular mechanisms is essential for identifying novel therapeutic targets. Recent discoveries have highlighted the ability of primary tumors to remotely regulate the microenvironment of candidate metastatic sites by transmitting specific signals; thus, the tumors create a “front station” conducive to tumor cell colonization, termed PMN, which acts to induce the early stage of tumor metastasis [9]. However, their precise role and mechanisms in gastric cancer peritoneal metastasis remain unclear. In this study, using clinical samples and immunocompetent mouse models, we demonstrated that METTL3-overexpressed gastric cancer is predisposed to peritoneal metastasis. Furthermore, we identified the critical role of tumor METTL3 in promoting exosome production and macrophage polarization, which contribute to the generation of an isPMN in the peritoneal cavity. We also explored potential therapeutic targets involved in initiating gastric cancer peritoneal metastasis.

Although gastric cancer peritoneal metastasis is the most challenging setting for treatment, current studies on peritoneal PMN are rare, likely due to the unique structural complexity of the peritoneum and the significant

expression in miR-17-92-overexpressed (miR17-92-oe) and control (vector) RAW 264.7 cells. $n = 3$ per group. (D-E) Cytokines produced by miR17-92-oe and control macrophages were detected using qPCR (D) and ELISA (E). (F-G) Influence of miR17-92-oe or control macrophages on T cell proliferation measured by CFSE fluorescence intensity (F) and on the CD8⁺/CD3⁺ ratio (G). $n = 3$ per group. (H-I) Influence of miR17-92-oe or control macrophages on T cell cytotoxicity against MFC cells detected by fluorescence density (H) and on the luciferase activity in surviving MFC cells (I). $n = 3$ per group. Asterisks indicate statistically significant differences at the corresponding time points in (I). (J) qPCR results of miR-17-92 cluster expression in exosomes with high miR-17-92 contents (miR17-92-oe-exo) and controls (vector-exo) derived from MFC cells. $n = 3$ per group. (K-L) Cytokine secretion from macrophages treated with miR17-92-oe-exo or control by qPCR (K) and ELISA (L). $n = 3$ per group. (M-P) Effects of miR17-92-oe-exo or control treated macrophages on T cell proliferation (M), CD8⁺/CD3⁺ T cell ratio (N) and MFC killing assessed by fluorescence density (O) or luciferase activity (P). $n = 3$ per group. Asterisks indicate significant differences between the miR17-92-oe-exo and the PBS groups at corresponding tumor-to-T-cell ratios in (P). (Q-U) Changes in tumor luciferase signal intensity (Q), abdominal circumferences (R), and body weights (S) in the MFC peritoneal metastasis model under miR17-92-oe-exo or vector-exo treatments, starting from peritoneal MFC injection, as well as the comparison of these parameters (T), and metastatic nodule numbers (U) on day 16. $n = 3$ per group. Asterisks indicate statistically significant differences at the corresponding time points in (Q-S). Data are presented as mean \pm standard deviation. ns, not significant; * $P < 0.05$; ** $P < 0.01$; *** $P < 0.001$. Abbreviation: CFSE, carboxyfluorescein succinimidyl ester; ELISA, enzyme-linked immunosorbent assay; exo, exosome; IntDen, integrated density; METTL3-cd, catalytically dead METTL3; METTL3-oe, METTL3-overexpressed; MFI, mean fluorescence intensity; miR17-92-oe, miR-17-92-overexpressed; PBS, phosphate buffered saline; qPCR, quantitative polymerase chain reaction; PMN, pre-metastatic niche; TGF- β , transforming growth factor- β ; TNF, tumor necrosis factor.

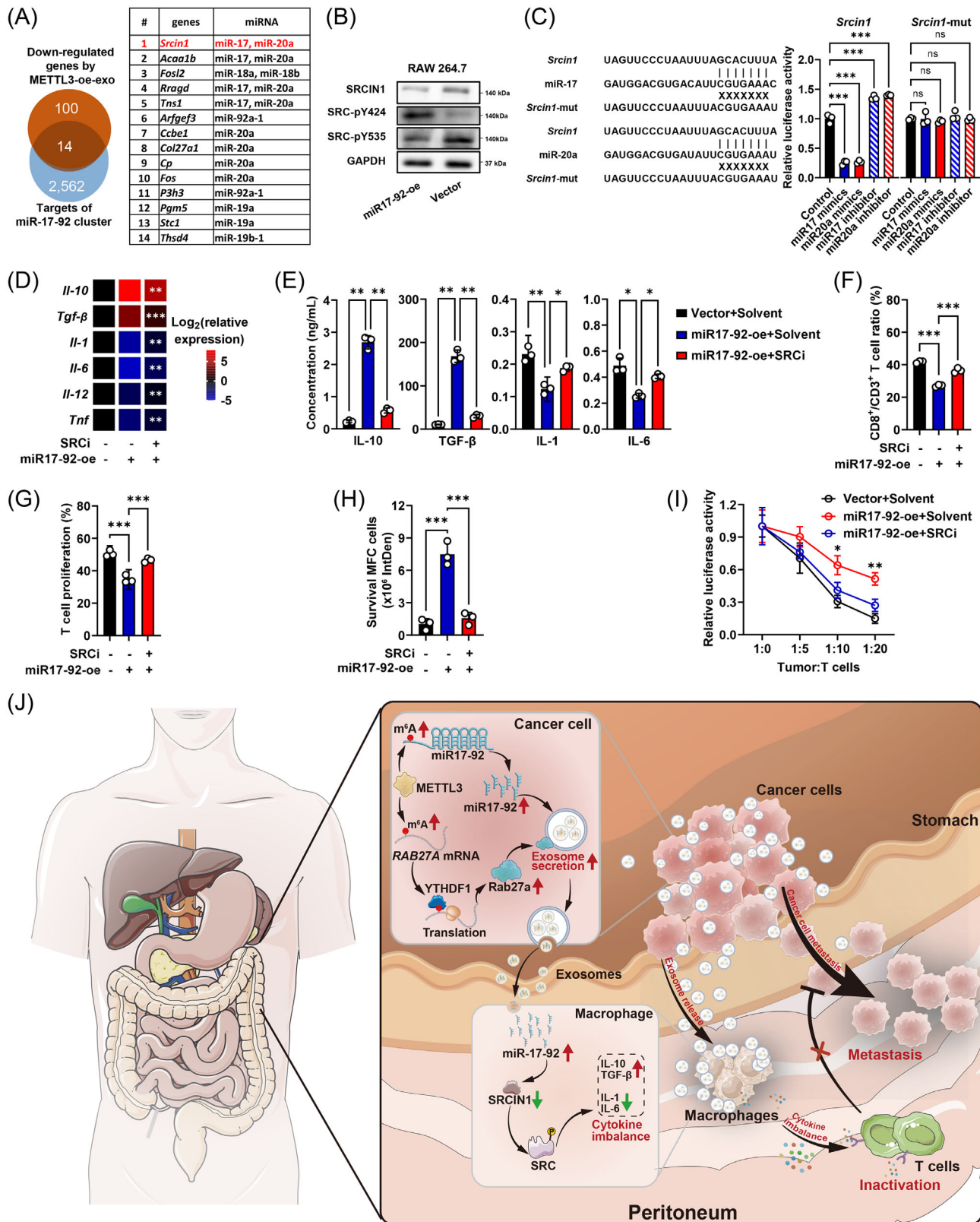


FIGURE 6 Exosomal miR-17-92 cluster modulated macrophages via the SRC pathway. (A) Overlaps between genes downregulated by exosomes from METTL3-overexpressed MFC cells (METTL3-oe-exo) in macrophages and tool-predicted targets of the miR-17-92 cluster. Venn diagram was on the left and overlapping genes were on the right. (B) Comparative analysis of SRCIN1 expression and SRC pathway activation in macrophages overexpressing miR-17-92 cluster (miR17-92-oe) and the control (vector), focusing on phosphorylation of tyrosine residues at the SRC activation site (Y424) and inhibitory site (Y535), corresponding to the sequence of P05480-1 in UniProt. (C) Validation of the

difficulty in obtaining clinical specimens compared to other metastatic sites [39]. This study revealed the existence of isPMN and its contribution to gastric cancer peritoneal metastasis in immunocompetent mice. This isPMN is characterized by an increased proportion of macrophages, anti-inflammatory conditions (i.e., with elevated anti-inflammatory cytokines and decreased pro-inflammatory factors) and reduced proportions of CD8⁺ T lymphocytes and their cytotoxicity. Notably, the peritoneal microenvironment is enriched with a large number of immune cells (including lymphocytes, monocytes, macrophages, and dendritic cells) that not only protect the peritoneal cavity from infection, but also participate in peripheral immunity [40]. Therefore, under physiological conditions, these immune cells theoretically provide immune surveillance that inhibits tumor cell invasion and colonization [41]. However, when modulated by distant primary gastric cancer cells, these immune factors are converted into a suppressive state, altering the local immune microenvironment to support the successful colonization of the gastric cancer cells that have arrived in the peritoneum, leading to peritoneal metastasis. These findings support further research into the immune properties of peritoneal PMN and the feasibility of targeting the peritoneal immune microenvironment early to prevent peritoneal metastasis of gastric cancer.

Subsequent studies identified macrophages as the central players in isPMN formation prior to gastric cancer peritoneal metastasis. Macrophages have been implicated in the metastasis of various tumors (such as colorectal cancer and pancreatic cancer [42]) as well as in the formation of PMN in multiple organs (including the lung [43], bone [44], and brain [45]). Although the enrichment of anti-inflammatory macrophages has been observed in gastric cancer peritoneal lesions [46–48], it remains unclear whether this enrichment is a cause or an outcome of gastric cancer peritoneal metastasis. In other words, it is unknown whether macrophages play a role in the initial stages of isPMN formation or not. Our research demon-

strated that exosome-educated macrophages helped establish an immunosuppressive microenvironment manifested by anti-immune cytokines and CD8⁺ T cell inactivation, whereas removal of peritoneal macrophages reversed this state and mitigated gastric cancer peritoneal metastasis. These findings highlight the critical role of macrophages in peritoneal PMN formation and demonstrate the feasibility of preventing gastric cancer peritoneal metastasis by inhibiting macrophage function.

Intriguingly, contrary to the inflammatory characteristics commonly observed in other studies [8], peritoneal PMN induced by METTL3-high gastric cancer appeared to function efficiently with reduced inflammatory cytokines, indicating that inflammation may not be essential for the METTL3-mediated peritoneal pre-metastatic microenvironment. Typically, inflammation occurs early during isPMN formation and recruits immunoregulatory cells [9]. Besides recruited cells, tissue-resident cells are another source of immunoregulatory cells during PMN formation [49]. We speculate that the rich reserve of peritoneal macrophages could serve as a source of immunoregulatory cells, thereby removing the need to recruit migratory immune cells via inflammation. This differs significantly from other tumor types or metastatic sites, making site-specific PMN highly conducive and “cost-effective” for gastric cancer peritoneal metastasis. This unique feature could enable us to identify a PMN before gastric cancer peritoneal metastasis occurs and aid in the development of targeted therapeutic strategies.

Tumor-derived exosomes can induce pro-tumor features of macrophages (including nuclear factor-kappa B (NF- κ B) activation, metabolic reprogramming, and PD-L1 upregulation) mediated by their abundant cargo content [50]. Our study highlights the critical role of METTL3-high cell-derived exosomes in mediating peritoneal isPMN, including fostering macrophage proliferation, modulating the imbalance between pro- and anti-inflammatory cytokine secretion, and subsequently inactivating CD8⁺ T lymphocytes. Notably, the current immune

inhibitory effects of miR-17 and miR-20a on SRCIN1 expression. Alignment of the 5'UTR of *Srcin1* with miRNAs is depicted on the left, with luciferase assay results on the right. $n = 3$ per group. (D-E) Cytokine profiles in macrophages overexpressing miR-17-92 cluster and treated with SRC inhibitor-1 (SRCi), assessed by quantitative PCR (D) and enzyme-linked immunosorbent assay (E). $n = 3$ per group. (F-G) Effects of SRC inhibition on T cell proliferation in presence of macrophages overexpressing miR-17-92 cluster, measured by CD8⁺/CD3⁺ T cell ratio (F) and CFSE fluorescence intensity (G). $n = 3$ per group. (H-I) Impact of SRC inhibition on T cell tumor killing in the presence of macrophages overexpressing miR-17-92 cluster, quantified by fluorescence intensity (H) and luciferase density (I) in surviving MFC cells. $n = 3$ per group. Asterisks indicate significant differences between miR17-92-oe + solvent and vector + solvent groups at corresponding tumor-to-T-cell ratios in (I). (J) Schematic representation of the role of METTL3-oe-exo miR-17-92 in macrophage polarization and cytokine disruption, contributing to the establishment of peritoneal PMN. Data are presented as mean \pm standard deviation. ns, not significant; * $P < 0.05$; ** $P < 0.01$; *** $P < 0.001$. Abbreviation: CFSE, carboxyfluorescein succinimidyl ester; METTL3-oe-exo, exosomes from METTL3-overexpressed cells; IntDen, integrated density; miR17-92-oe, miR-17-92-overexpressed; PMN, pre-metastatic niche; pY, phosphorylated tyrosine; SRCi, SRC inhibitor-1; SRCIN1, SRC kinase signaling inhibitor 1; TGF- β , transforming growth factor- β ; TNF, tumor necrosis factor; UTR, untranslated region.

microenvironment is reprogrammed mainly by secreted inhibitory inflammatory factors rather than by altering the common membrane markers of M1/M2 polarization (CD86 and CD206) [51]. Given the close interaction between exosomes and macrophages, both are indispensable for the formation of peritoneal isPMN and the promotion of peritoneal metastasis. Therefore, targeting exosomes may be an important strategy for reversing the progression of peritoneal PMN.

Regulation of exosome secretion by METTL3 from gastric cancer cells represents another vital initiating step in PMN development. METTL3 is a multifaceted driver of tumor pathogenesis, including cell proliferation, apoptosis resistance, invasion, metastasis, angiogenesis, and metabolic dysregulation [52]. Recent studies have shown that METTL3 modulates the immunosuppressive microenvironment by enhancing the translation of mRNAs involved in cholesterol biosynthesis, which in turn suppresses CD8⁺ T lymphocytes and promotes the recruitment and polarization of tumor-associated macrophages and MDSCs [53]. In contrast to these studies, our study highlights METTL3's distinct ability to transform the distant peritoneum into an isPMN state to facilitate peritoneal metastasis. This finding extends the regulatory reach of tumor METTL3 and highlights its dependence on exosome mediation.

A function of METTL3 identified in this study is the control of exosome secretion and content. Specifically, METTL3 facilitated exosome biogenesis by upregulating RAB27A expression under YTHDF1 recognition of the m⁶A modification of the A502 locus of RAB27A mRNA. In addition, METTL3 regulates exosomal components, particularly miRNAs. Considering the facilitation of miR-17-92 biogenesis in tumor cells by METTL3 and the observed increase of all miRNA cluster members within exosomes [15], it is plausible that these miRNAs are passively packaged into exosomes. Furthermore, the miR-17-92 cluster is the key exosomal miRNA responsible for the activation of pro-PMN macrophages. This cluster has been well-documented as a potent immune regulator that inhibits macrophage inflammatory cytokine production [54] and induces immune suppression [55]. However, it is worth noting that previous studies primarily focused on the intracellular miR-17-92 cluster rather than on those derived from exosomes. In particular, our results emphasize the significant contribution of exosomal miR-17-92 in mediating peritoneal PMN formation in gastric cancer metastasis, mainly by targeting SRCIN1, which is consistent with previous reports [56]. The SRC pathway is a well-recognized modulator of macrophage-induced inflammatory responses, which may explain the regulatory effect of exosomal miR-17-92 on macrophage function in a peritoneal metastasis model of gastric cancer.

This study revealed the mechanism by which METTL3 regulates the secretion of miR-17-92 cluster-enriched exosomes by gastric cancer cells, reprograms the peritoneal microenvironment into a macrophage-dominated isPMN, and promotes peritoneal metastasis. These findings suggest that components at any level of this long regulatory axis hold promise as potential biomarkers and therapeutic targets for controlling gastric cancer peritoneal metastasis. METTL3 expression in primary gastric cancer can be used either independently or in combination with other indicators (such as peritoneal fluid cytology or radiomics) to assess the risk of peritoneal metastasis and to tailor treatment strategies [57]. Given the high stability of nucleic acids within exosomes [58], the detection of exosomal miR-17-92 in ascites or peripheral blood may also serve as a predictor of peritoneal PMN formation and forthcoming metastasis. In terms of therapeutic intervention, the link between m⁶A modification and exosomes allows for the inhibition of exosomes by targeting upstream regulators (such as METTL3 or YTHDF1) to counteract tumor growth, metastasis, and drug resistance [59], especially as exosome inhibitors (such as GW4869) have not received clinical approval according to clinicaltrials.gov. Notably, we have previously demonstrated that intrinsic METTL3 promotes gastric cancer cell growth and invasion [15], which does not interfere with METTL3's role in promoting PMN formation in this study. Thus, targeting METTL3 may offer a dual benefit by impeding primary tumor progression and reversing peritoneal isPMN formation, offering a promising approach for preventing gastric cancer peritoneal metastasis. Currently, the METTL3 inhibitor STM2457 is undergoing early-phase clinical trials [60], making METTL3 a druggable target of great significance in gastric cancer treatment. Given the well-known oncogenic role of miR-17-92, targeting this miRNA cluster with MIR17HG primary transcript inhibitor (MIR17PTi) represents another promising approach to prevent gastric cancer peritoneal metastasis [61].

This study's limitations relate to the clinical analyses. First, the cohorts used were relatively small, which may reduce the statistical power of our findings and introduce potential bias. Second, due to the limited availability of ascites from healthy individuals or gastric cancer patients without peritoneal metastasis, cirrhotic ascites were used as controls. These limitations underscore the need for validation in larger, prospective cohorts.

5 | CONCLUSIONS

In summary, as illustrated in Figure 6J, METTL3 enhanced gastric cancer exosome biogenesis by facilitating RAB27A mRNA translation and increasing miR-17-92 cargo, which

induced an immunosuppressive phenotype in distant peritoneal macrophages and contributed to iSPMN formation and subsequent peritoneal metastasis. Understanding the key molecular mechanisms underlying gastric cancer peritoneal metastasis brings us closer to effective prevention and intervention of this challenging clinical problem.

AUTHOR CONTRIBUTIONS

Lian Liu and Song Li conceived and designed the study. Jianyuan Zhou and Qian Yang performed most of the *in vitro* experiments. Qian Yang and Shuang Wang performed the *in vivo* studies. Jianyuan Zhou, Shuang Wang, and Qian Yang analyzed the clinical and omics data. Shulun Nie, Chunwang Ji, and Jiahui Chu helped with the *in vivo* studies. Xue Zhang, Shuhan Li, Xuanyu Zhou, Xuehui Wu, Jianqiao Jiao, Ruitao Xu, Qian Xu, Miao Huang, Qiushi Wang, Liliang Dou, Qinqin Hu, Fan Jiang, Xin Dai, Zhaodi Nan, Xinyu Song, and Di Zhang helped the *in vitro* experiments. Lian Liu, Song Li, Jianyuan Zhou, and Shuang Wang analyzed the data and drafted the manuscript. All authors have read and approved the final manuscript.

ACKNOWLEDGMENTS

The 293T cells were generously provided by the Xie Jianjun Lab at Shantou University (Guangdong, P. R. China). We thank Dr. Duanbo Shi and Dr. Mei Qi at Shandong University Qilu Hospital for their assistance with the review of pathological slides. The manuscript was edited by Alexandra H. Marshall from Marshall Medical Communications. This study was supported by the National Natural Science Foundation of China (grant number, 82173305) and the Natural Science Foundation of Shandong Province (grant number, ZR2023LSW018).

CONFLICT OF INTEREST STATEMENT

The authors have no competing interests.

ETHICS APPROVAL AND CONSENT TO PARTICIPATE

Studies involving human samples were approved by the Medical Ethical Committee of Shandong University Qilu Hospital (No. KYLL-2018214) and the Ethics Committee for Scientific Research of Shandong University Qilu Hospital (No. KYLL-202111-144 and KYLL-2024-07011-1). Written informed consent for participation was obtained from all participants. Animal studies were approved by the Ethics Committee on Animal Experiments of Shandong University Qilu Hospital (No. DWLL-2022-069) and complied with the ARRIVE guidelines.

DATA AVAILABILITY STATEMENT

The GSE166972, GSE66229, GSE239676, and GSE237876 datasets were accessed from the Gene Expression Omnibus (<https://www.ncbi.nlm.nih.gov/geo/>). The EGAD00001006172 dataset was obtained from the European Genome-Phenome Archive (<https://ega-archive.org>). Transcriptome data for the TCGA STAD cohort were obtained from the Xena database (<https://xena.ucsc.edu/public>). The raw sequencing data generated in this study have been deposited in publicly accessible databases; RNA-seq data are deposited in the Genome Sequence Archive database [<https://ngdc.cncb.ac.cn/gsa>] under accession number CRA022142, exosomal miRNA sequencing data in the Sequence Read Archive [<https://www.ncbi.nlm.nih.gov/sra>] database under accession number SRS23827005, and proteomic data in the Open Archive for Miscellaneous Data database [<https://ngdc.cncb.ac.cn/omix/>] under accession number OMIX008665. All other data supporting the results of this study are available from the corresponding author upon reasonable request.

ORCID

Lian Liu  <https://orcid.org/0000-0001-5868-4482>

REFERENCES

- Sung H, Ferlay J, Siegel RL, Laversanne M, Soerjomataram I, Jemal A, et al. Global Cancer Statistics 2020: GLOBOCAN Estimates of Incidence and Mortality Worldwide for 36 Cancers in 185 Countries. *CA Cancer J Clin.* 2021;71(3):209–49.
- Dixon M, Mahar AL, Helyer LK, Vasilevska-Ristovska J, Law C, Coburn NG. Prognostic factors in metastatic gastric cancer: results of a population-based, retrospective cohort study in Ontario. *Gastric Cancer.* 2016;19(1):150–9.
- Kwee RM, Kwee TC. Modern imaging techniques for preoperative detection of distant metastases in gastric cancer. *World J Gastroenterol.* 2015;21(37):10502–9.
- Kang D, Kim IH. Molecular Mechanisms and Potential Rationale of Immunotherapy in Peritoneal Metastasis of Advanced Gastric Cancer. *Biomedicines.* 2022;10(6):1376.
- Gwee YX, Chia DKA, So J, Ceelen W, Yong WP, Tan P, et al. Integration of Genomic Biology Into Therapeutic Strategies of Gastric Cancer Peritoneal Metastasis. *J Clin Oncol.* 2022;40(24):2830.
- Ji ZH, Yu Y, Liu G, Zhang YB, An SL, Li B, et al. Peritoneal cancer index (PCI) based patient selecting strategy for complete cytoreductive surgery plus hyperthermic intraperitoneal chemotherapy in gastric cancer with peritoneal metastasis: A single-center retrospective analysis of 125 patients. *Eur J Surg Oncol.* 2021;47(6):1411–9.
- Peinado H, Zhang H, Matei IR, Costa-Silva B, Hoshino A, Rodrigues G, et al. Pre-metastatic niches: organ-specific homes for metastases. *Nat Rev Cancer.* 2017;17(5):302–17.
- Liu Y, Cao X. Characteristics and Significance of the Pre-metastatic Niche. *Cancer Cell.* 2016;30(5):668–81.

9. Patras L, Shaashua L, Matei I, Lyden D. Immune determinants of the pre-metastatic niche. *Cancer Cell*. 2023;41(3):546–72.
10. McAllister SS, Weinberg RA. The tumour-induced systemic environment as a critical regulator of cancer progression and metastasis. *Nat Cell Biol*. 2014;16(8):717–27.
11. Guo L, Zhu Y, Li L, Zhou S, Yin G, Yu G, et al. Breast cancer cell-derived exosomal miR-20a-5p promotes the proliferation and differentiation of osteoclasts by targeting SRCIN1. *Cancer Med*. 2019;8(12):5687–701.
12. Kalluri R. The biology and function of exosomes in cancer. *J Clin Invest*. 2016;126(4):1208–15.
13. Gao J, Li S, Xu Q, Zhang X, Huang M, Dai X, et al. Exosomes Promote Pre-Metastatic Niche Formation in Gastric Cancer. *Front Oncol*. 2021;11:652378.
14. Yue SW, Liu HL, Su HF, Luo C, Liang HF, Zhang BX, et al. m6A-regulated tumor glycolysis: new advances in epigenetics and metabolism. *Mol Cancer*. 2023;22(1):137.
15. Sun Y, Li S, Yu W, Zhao Z, Gao J, Chen C, et al. N(6)-methyladenosine-dependent pri-miR-17-92 maturation suppresses PTEN/TMEM127 and promotes sensitivity to everolimus in gastric cancer. *Cell Death Dis*. 2020;11(10):836.
16. Xie JW, Huang XB, Chen QY, Ma YB, Zhao YJ, Liu LC, et al. m(6)A modification-mediated BATF2 acts as a tumor suppressor in gastric cancer through inhibition of ERK signaling. *Mol Cancer*. 2020;19(1):114.
17. Zhang Y, Qiu JG, Jia XY, Ke Y, Zhang MK, Stieg D, et al. METTL3-mediated N6-methyladenosine modification and HDAC5/YY1 promote IFFO1 downregulation in tumor development and chemo-resistance. *Cancer Lett*. 2023;553:215971.
18. Zou S, Chen S, Rao G, Zhang G, Ma M, Peng B, et al. Extrachromosomal circular MiR-17-92 amplicon promotes HCC. *Hepatology*. 2024;79(1):79–95.
19. Shen DD, Pang JR, Bi YP, Zhao LF, Li YR, Zhao LJ, et al. LSD1 deletion decreases exosomal PD-L1 and restores T-cell response in gastric cancer. *Mol Cancer*. 2022;21(1):75.
20. Zhu X, Zheng W, Wang X, Li Z, Shen X, Chen Q, et al. Enhanced Photodynamic Therapy Synergizing with Inhibition of Tumor Neutrophil Ferroptosis Boosts Anti-PD-1 Therapy of Gastric Cancer. *Adv Sci (Weinh)*. 2024;11(12):e2307870.
21. Pinto A, Marangon I, Mereaux J, Nicolas-Boluda A, Lavieu G, Wilhelm C, et al. Immune Reprogramming Precision Photodynamic Therapy of Peritoneal Metastasis by Scalable Stem-Cell-Derived Extracellular Vesicles. *ACS Nano*. 2021;15(2):3251–63.
22. Li M, Ye J, Xia Y, Li M, Li G, Hu X, et al. METTL3 mediates chemoresistance by enhancing AML homing and engraftment via ITGA4. *Leukemia*. 2022;36(11):2586–95.
23. Percie du Sert N, Hurst V, Ahluwalia A, Alam S, Avey MT, Baker M, et al. The ARRIVE guidelines 2.0: Updated guidelines for reporting animal research. *PLoS Biol*. 2020;18(7):e3000410.
24. De Jesus A, Pusec CM, Nguyen T, Keyhani-Nejad F, Gao P, Weinberg SE, et al. Optimized protocol to isolate primary mouse peritoneal macrophage metabolites. *STAR Protoc*. 2022;3(4):101668.
25. Liao Y, Smyth GK, Shi W. featureCounts: an efficient general purpose program for assigning sequence reads to genomic features. *Bioinformatics*. 2014;30(7):923–30.
26. Love MI, Huber W, Anders S. Moderated estimation of fold change and dispersion for RNA-seq data with DESeq2. *Genome Biol*. 2014;15(12):550.
27. Yu G, Wang LG, Han Y, He QY. clusterProfiler: an R package for comparing biological themes among gene clusters. *OMICS*. 2012;16(5):284–7.
28. Wang L, Feng Z, Wang X, Wang X, Zhang X. DEGseq: an R package for identifying differentially expressed genes from RNA-seq data. *Bioinformatics*. 2010;26(1):136–8.
29. Sturm G, Finotello F, List M. Immunedeconv: An R Package for Unified Access to Computational Methods for Estimating Immune Cell Fractions from Bulk RNA-Sequencing Data. *Methods Mol Biol*. 2020;2120:223–32.
30. Chen B, Khodadoust MS, Liu CL, Newman AM, Alizadeh AA. Profiling Tumor Infiltrating Immune Cells with CIBERSORT. *Methods Mol Biol*. 2018;1711:243–59.
31. Quan F, Liang X, Cheng M, Yang H, Liu K, He S, et al. Annotation of cell types (ACT): a convenient web server for cell type annotation. *Genome Med*. 2023;15(1):91.
32. Wang R, Dang M, Harada K, Han G, Wang F, Pool Pizzi M, et al. Single-cell dissection of intratumoral heterogeneity and lineage diversity in metastatic gastric adenocarcinoma. *Nat Med*. 2021;27(1):141–51.
33. Li Q, Li B, Li Q, Wei S, He Z, Huang X, et al. Exosomal miR-21-5p derived from gastric cancer promotes peritoneal metastasis via mesothelial-to-mesenchymal transition. *Cell Death Dis*. 2018;9(9):854.
34. Xia X, Zhang Z, Zhu C, Ni B, Wang S, Yang S, et al. Neutrophil extracellular traps promote metastasis in gastric cancer patients with postoperative abdominal infectious complications. *Nat Commun*. 2022;13(1):1017.
35. Zhou W, Woodson M, Sherman MB, Neelakanta G, Sultana H. Exosomes mediate Zika virus transmission through SMPD3 neutral Sphingomyelinase in cortical neurons. *Emerg Microbes Infect*. 2019;8(1):307–26.
36. Singh R, Pochampally R, Watabe K, Lu Z, Mo YY. Exosome-mediated transfer of miR-10b promotes cell invasion in breast cancer. *Mol Cancer*. 2014;13:256.
37. Chen L, Guo P, He Y, Chen Z, Chen L, Luo Y, et al. HCC-derived exosomes elicit HCC progression and recurrence by epithelial-mesenchymal transition through MAPK/ERK signalling pathway. *Cell Death Dis*. 2018;9(5):513.
38. Wang G, Li J, Bojmar L, Chen H, Li Z, Tobias GC, et al. Tumour extracellular vesicles and particles induce liver metabolic dysfunction. *Nature*. 2023;618(7964):374–82.
39. Costa-Silva B, Aiello NM, Ocean AJ, Singh S, Zhang H, Thakur BK, et al. Pancreatic cancer exosomes initiate pre-metastatic niche formation in the liver. *Nat Cell Biol*. 2015;17(6):816–26.
40. Okabe Y. Immune Niche Within the Peritoneal Cavity. *Curr Top Microbiol Immunol*. 2021;434:123–34.
41. Bootsma S, Bijlsma MF, Vermeulen L. The molecular biology of peritoneal metastatic disease. *EMBO Mol Med*. 2023;15(3):e15914.
42. Griesmann H, Drexel C, Milosevic N, Sipos B, Rosendahl J, Gress TM, et al. Pharmacological macrophage inhibition decreases metastasis formation in a genetic model of pancreatic cancer. *Gut*. 2017;66(7):1278–85.
43. Hongu T, Pein M, Insua-Rodriguez J, Gutjahr E, Mattavelli G, Meier J, et al. Perivascular tenascin C triggers sequential activation of macrophages and endothelial cells to generate a pro-metastatic vascular niche in the lungs. *Nat Cancer*. 2022;3(4):486–504.

44. Lu X, Kang Y. Chemokine (C-C motif) ligand 2 engages CCR2+ stromal cells of monocytic origin to promote breast cancer metastasis to lung and bone. *J Biol Chem*. 2009;284(42):29087–96.
45. Xing F, Liu Y, Wu SY, Wu K, Sharma S, Mo YY, et al. Loss of XIST in Breast Cancer Activates MSN-c-Met and Reprograms Microglia via Exosomal miRNA to Promote Brain Metastasis. *Cancer Res*. 2018;78(15):4316–30.
46. Eum HH, Kwon M, Ryu D, Jo A, Chung W, Kim N, et al. Tumor-promoting macrophages prevail in malignant ascites of advanced gastric cancer. *Exp Mol Med*. 2020;52(12):1976–88.
47. Takahashi K, Kurashina K, Yamaguchi H, Kanamaru R, Ohzawa H, Miyato H, et al. Altered intraperitoneal immune microenvironment in patients with peritoneal metastases from gastric cancer. *Front Immunol*. 2022;13:969468.
48. Yamaguchi T, Fushida S, Yamamoto Y, Tsukada T, Kinoshita J, Oyama K, et al. Tumor-associated macrophages of the M2 phenotype contribute to progression in gastric cancer with peritoneal dissemination. *Gastric Cancer*. 2016;19(4):1052–65.
49. Aegerter H, Lambrecht BN, Jakubzick CV. Biology of lung macrophages in health and disease. *Immunity*. 2022;55(9):1564–80.
50. Morrissey SM, Zhang F, Ding C, Montoya-Durango DE, Hu X, Yang C, et al. Tumor-derived exosomes drive immunosuppressive macrophages in a pre-metastatic niche through glycolytic dominant metabolic reprogramming. *Cell Metab*. 2021;33(10):2040–58 e10.
51. Xu F, Cui WQ, Wei Y, Cui J, Qiu J, Hu LL, et al. Astragaloside IV inhibits lung cancer progression and metastasis by modulating macrophage polarization through AMPK signaling. *J Exp Clin Cancer Res*. 2018;37(1):207.
52. Wang L, Hui H, Agrawal K, Kang Y, Li N, Tang R, et al. m(6) A RNA methyltransferases METTL3/14 regulate immune responses to anti-PD-1 therapy. *EMBO J*. 2020;39(20):e104514.
53. Pan Y, Chen H, Zhang X, Liu W, Ding Y, Huang D, et al. METTL3 drives NAFLD-related hepatocellular carcinoma and is a therapeutic target for boosting immunotherapy. *Cell Rep Med*. 2023;4(8):101144.
54. Lai L, Song Y, Liu Y, Chen Q, Han Q, Chen W, et al. MicroRNA-92a negatively regulates Toll-like receptor (TLR)-triggered inflammatory response in macrophages by targeting MKK4 kinase. *J Biol Chem*. 2013;288(11):7956–67.
55. Kuo G, Wu CY, Yang HY. MiR-17-92 cluster and immunity. *J Formos Med Assoc*. 2019;118(1 Pt 1):2–6.
56. Zhao X, Xu Y, Sun X, Ma Y, Zhang Y, Wang Y, et al. miR-17-5p promotes proliferation and epithelial-mesenchymal transition in human osteosarcoma cells by targeting SRC kinase signaling inhibitor 1. *J Cell Biochem*. 2019;120(4):5495–504.
57. Dong D, Tang L, Li ZY, Fang MJ, Gao JB, Shan XH, et al. Development and validation of an individualized nomogram to identify occult peritoneal metastasis in patients with advanced gastric cancer. *Ann Oncol*. 2019;30(3):431–8.
58. Wang W, Yue C, Gao S, Li S, Zhou J, Chen J, et al. Promising Roles of Exosomal microRNAs in Systemic Lupus Erythematosus. *Front Immunol*. 2021;12:757096.
59. Xi Y, Shen Y, Chen L, Tan L, Shen W, Niu X. Exosome-mediated metabolic reprogramming: Implications in esophageal carcinoma progression and tumor microenvironment remodeling. *Cytokine Growth Factor Rev*. 2023;73:78–92.
60. Yankova E, Blackaby W, Albertella M, Rak J, De Braekeleer E, Tsagkogeorga G, et al. Small-molecule inhibition of METTL3 as a strategy against myeloid leukaemia. *Nature*. 2021;593(7860):597–601.
61. Morelli E, Biamonte L, Federico C, Amodio N, Di Martino MT, Gallo Cantafio ME, et al. Therapeutic vulnerability of multiple myeloma to MIR17PTi, a first-in-class inhibitor of pri-miR-17-92. *Blood*. 2018;132(10):1050–63.

SUPPORTING INFORMATION

Additional supporting information can be found online in the Supporting Information section at the end of this article.

How to cite this article: Li S, Zhou J, Wang S, Yang Q, Nie S, Ji C, et al. N⁶-methyladenosine-regulated exosome biogenesis orchestrates an immunosuppressive pre-metastatic niche in gastric cancer peritoneal metastasis. *Cancer Commun*. 2025;1–25. <https://doi.org/10.1002/cac2.70034>